

Efficient and accurate nonlinear model reduction via first-order empirical interpolation

Ngoc Cuong Nguyen^a, Jaime Peraire^a

^a*Center for Computational Engineering, Department of Aeronautics and Astronautics, Massachusetts Institute of Technology, 77 Massachusetts Avenue, Cambridge, MA, 02139, USA*

Abstract

We present a model reduction approach that extends the original empirical interpolation method to enable accurate and efficient reduced basis approximation of parametrized nonlinear partial differential equations (PDEs). In the presence of nonlinearity, the Galerkin reduced basis approximation remains computationally expensive due to the high complexity of evaluating the nonlinear terms, which depends on the dimension of the truth approximation. The empirical interpolation method (EIM) was proposed as a nonlinear model reduction technique to render the complexity of evaluating the nonlinear terms independent of the dimension of the truth approximation. We introduce a first-order empirical interpolation method (FOEIM) that makes use of the partial derivative information to construct an inexpensive and stable interpolation of the nonlinear terms. We propose two different FOEIM algorithms to generate interpolation points and basis functions. We apply the FOEIM to nonlinear elliptic PDEs and compare it to the Galerkin reduced basis approximation and the EIM. Numerical results are presented to demonstrate the performance of the three reduced basis approaches.

Keywords: empirical interpolation method, reduced basis method, model reduction, finite element method, elliptic equations, reduced order model

1. Introduction

Many physical systems in engineering and science are described by partial differential equations (PDEs). The design, optimization, control, and characterization of physical systems often require repeated, accurate and fast prediction of quantities of interest (QoIs). The evaluation of QoIs demands

numerical approximation of the underlying PDE by finite element (FE), finite difference (FD) and finite volume (FV) methods. The numerical approximation of PDEs yields high-dimensional systems of equations — known as full order models (FOMs) — which can be computationally expensive for complex physical processes. Model reduction methods seek to reduce the computational complexity of FOMs by constructing reduced order models (ROMs) in significantly lower dimensional spaces. Projection-based model reduction techniques have been widely used to construct ROMs in numerous applications such as fluid mechanics [1, 2, 3, 4, 5, 6, 7, 8, 9, 10, 11], solid mechanics [12, 13, 14, 15, 16], electromagnetic [17, 18, 19], optimization [20, 21], inverse problems [22, 23, 24, 25], multiscale problems [26], optimal control [27, 28], and data assimilation [29, 30, 31]. The success of projection-based ROMs without hyper-reduction is limited to FOMs with affine parameter dependence [12, 32] and low-order polynomial nonlinearities [3, 33]. In these cases, very efficient ROMs can be developed by resolving the affine and non-linear terms into the sum of products of the basis functions and coefficients.

In the presence of strong nonlinearities, projection-based ROMs become computationally expensive without an efficient treatment of the nonlinear terms [34, 35]. A number of different approaches have been developed to deal with nonlinear PDEs in the context of model reduction. One approach is linearization [36] and polynomial approximation [37]. However, inefficient representation of the nonlinear terms and fast exponential growth (with the degree of the nonlinear approximation order) of the computational complexity render these methods quite expensive, in particular for strong nonlinearities.¹ Another approach uses piecewise polynomials to approximate nonlinear terms [38]. However, there are still many nonlinear functions that may not be approximated well by using low degree piecewise polynomials unless there are very many constituent polynomials.

An efficient model reduction technique for PDEs with nonaffine parameter dependence was first proposed in [39] that led to the development of the empirical interpolation method for constructing coefficient-function ap-

¹This refers to the presence of high-order polynomial or non-polynomial nonlinearities in the parametrized PDEs. Typically, q -degree polynomial terms result in $O(N^{q+1})$ operation count to assemble the reduced model due to the expansion of the nonlinear terms into the sum of products of the basis functions and coefficients. Here N is the dimension of the reduced model. Non-polynomial terms may not be admitted to such expansion and may lead to a higher computational cost that depends on the dimension of the full model.

proximation of nonaffine terms. Shortly later, the empirical interpolation method was extended to develop efficient ROMs for nonlinear PDEs [34]. Since the pioneer work [39], the EIM has been widely used to construct efficient ROMs of nonaffine and nonlinear PDEs for different applications [34, 40, 41, 20, 42, 43, 44]. In [45], the best-points interpolation method (BPIM) was developed to treat nonlinearity in FOMs and generate efficient ROMs for elliptic problems and convection-diffusion problems. In [24], gappy POD, EIM, and BPIM were applied to a nonlinear combustion problem governed by an advection-diffusion-reaction PDE to enable the rapid solution of large-scale statistical inverse problems. In [46], a lifting transformation method was proposed to reduce the complexity of evaluating nonlinear reduced order models. A new model reduction method for parametrized nonlinear PDEs is recently introduced in [47] to provide rapid evaluation of the nonlinear reduced order model via an empirical quadrature procedure. This method differs from the interpolation-then-integration approaches described earlier because it employs the sparse quadrature rules to directly approximate the nonlinear integrals.

The discrete empirical interpolation method (DEIM) [48] is a discrete variant of the empirical interpolation method. DEIM consider a collection of vectors arising from the spatial discretization of parameter-dependent functions or PDEs and select a subset of vectors and associated interpolation indices. DEIM has also been widely used to construct efficient ROMs of nonlinear PDEs [49, 16, 8, 46]. DEIM is closely related to missing point estimation [50] in the sense that both methods employ a small selected set of spatial grid points to avoid evaluation of the expensive inner products at every time step that are required to evaluate the nonlinearities. However, ROMs via (D)EIM have been shown to suffer from instabilities in certain situations [51]. Adaptation [52] and localization [53] of the low-dimensional subspaces have been proposed to improve the stability of ROMs via empirical interpolation. Oversampling uses more interpolation points than basis functions so that the nonlinear terms are approximated via least-squares regression rather than via interpolation [51]. Oversampling methods such as gappy POD [54, 55], missing point estimation [50, 56], Gauss-Newton with approximated tensors [10], and generalized EIM (GEIM) [57] can provide more stable and accurate approximations than empirical interpolation especially when the samples are perturbed due to noise turbulence, and numerical inaccuracies.

The original empirical interpolation method (EIM) [39, 34] was proposed

as an efficient model reduction technique to render the complexity of evaluating the nonlinear terms independent of the dimension of the truth approximation. The main idea is to replace any nonlinear term with a reduced basis expansion expressed as a linear combination of pre-computed basis functions and parameter-dependent coefficients. The coefficients are determined efficiently by an inexpensive and stable interpolation procedure. In the empirical interpolation method, the basis functions are instances of the nonlinear function at N parameter points in a sample set S_N . Therefore, the number of basis functions and interpolation points can not exceed N . In order to improve the approximation accuracy, we must increase N at the expense of increasing the offline cost because we need to evaluate the FOM for all parameter points in S_N .

We seek to improve the accuracy without increasing the size of the sample set. To this end, we employ the partial derivatives of the nonlinear function evaluated at parameter points in S_N to construct additional interpolating functions and interpolation points. The resulting method is called the first-order empirical interpolation method (FOEIM) to distinguish itself from the EIM that does not use first-order partial derivatives. The proposed method is applied to nonlinear elliptic PDEs and compared to both the Galerkin reduced basis approximation and the EIM. Numerical results are presented to assess the performance of the three reduced basis approaches.

Indeed, Hermitian spaces built upon sensitivity derivatives of the field variable with respect to the parameter [58] or, more generally, Lagrange-Hermitian spaces [59] were long considered for the RB approximation of parametrized PDEs. We emphasize that our method does not require *sensitivity* derivatives of the field variable with respect to the parameters, which are often more expensive to compute than the field variable itself because they are obtained by differentiating the underlying PDEs with respect to the parameters and solving the resulting PDEs. In fact, our method requires *partial* derivatives of the nonlinear terms with respect to the field variable and the parameters, which are inexpensive to compute if the field variable is already computed. This is because evaluating the partial derivatives of the nonlinear terms has a similar cost as evaluating the nonlinear terms.

The paper is organized as follows. In Section 2, we introduce the first-order empirical interpolation method. The model problem, reduced basis approximations, and computational considerations for nonlinear elliptic problems and nonlinear diffusion equations are then discussed in Sections 3 and 4, respectively. Numerical results are included in each section in order to

assess our method. Finally, in Section 5, we make a number of concluding remarks on the results as well as future work.

2. First-order empirical interpolation

2.1. The interpolation problem

Let $\Omega \subset \mathbb{R}^d$ be the physical domain in which the spatial point \mathbf{x} resides. Let $\mathcal{D} \subset \mathbb{R}^P$ be the parameter domain in which our P -tuple parameter point $\boldsymbol{\mu}$ resides. Let $u(\mathbf{x}, \boldsymbol{\mu}) \in L^\infty(\Omega \times \mathcal{D})$ be a parameter-dependent function of sufficient regularity. We consider the problem of approximating a nonlinear function $g(u(\mathbf{x}, \boldsymbol{\mu}), \boldsymbol{\mu})$ by a reduced basis expansion $g_M(\mathbf{x}, \boldsymbol{\mu})$, where $g(u, \boldsymbol{\mu})$ is generally nonlinear with respect to the first argument. We assume that the partial derivatives, $g'_u(u, \boldsymbol{\mu}) \equiv \partial g(u, \boldsymbol{\mu})/\partial u$ and $g'_\mu(u, \boldsymbol{\mu}) \equiv \partial g(u, \boldsymbol{\mu})/\partial \boldsymbol{\mu}$, are bounded everywhere in $\Omega \times \mathcal{D}$.

We assume that we are given a set of interpolating functions $W_M^g = \text{span}\{\psi_m(\mathbf{x}), 1 \leq m \leq M\}$ and a set of interpolation points $T_M = \{\hat{\mathbf{x}}_1, \dots, \hat{\mathbf{x}}_M\}$. The RB expansion $g_M(\mathbf{x}, \boldsymbol{\mu})$ is expressed as

$$g_M(\mathbf{x}, \boldsymbol{\mu}) = \sum_{m=1}^M \beta_{M,m}(\boldsymbol{\mu}) \psi_m(\mathbf{x}), \quad (1)$$

where the coefficients $\beta_{M,m}(\boldsymbol{\mu}), 1 \leq m \leq M$, are found as the solution of the following linear system

$$\sum_{m=1}^M \psi_m(\hat{\mathbf{x}}_k) \beta_{M,m}(\boldsymbol{\mu}) = g(u(\hat{\mathbf{x}}_k, \boldsymbol{\mu}), \boldsymbol{\mu}), \quad 1 \leq k \leq M. \quad (2)$$

It is convenient to compute the coefficient vector $\boldsymbol{\beta}_M(\boldsymbol{\mu})$ as follows

$$\boldsymbol{\beta}_M(\boldsymbol{\mu}) = \mathbf{B}_M^{-1} \mathbf{b}_M(\boldsymbol{\mu}), \quad (3)$$

where $\mathbf{B}_M \in \mathbb{R}^{M \times M}$ has entries $B_{M,km} = \psi_m(\hat{\mathbf{x}}_k)$ and $\mathbf{b}_M(\boldsymbol{\mu}) \in \mathbb{R}^M$ has entries $b_{M,k}(\boldsymbol{\mu}) = g(u(\hat{\mathbf{x}}_k, \boldsymbol{\mu}), \boldsymbol{\mu})$. Since $g_M(\hat{\mathbf{x}}_k, \boldsymbol{\mu}) = g(\hat{\mathbf{x}}_k, \boldsymbol{\mu}), 1 \leq k \leq M$, the RB expansion $g_M(\cdot, \boldsymbol{\mu})$ is an interpolant of $g(\cdot, \boldsymbol{\mu})$ over M interpolation points. We define the associated error as

$$\varepsilon_M(\boldsymbol{\mu}) = \|g(u(\mathbf{x}, \boldsymbol{\mu}), \boldsymbol{\mu}) - g_M(\mathbf{x}, \boldsymbol{\mu})\|_{L^\infty(\Omega)}, \quad (4)$$

which is a measure of the approximation accuracy for any given $\boldsymbol{\mu} \in \mathcal{D}$. The complexity of computing the coefficient vector $\boldsymbol{\beta}_M(\boldsymbol{\mu})$ in (3) for any given $\boldsymbol{\mu}$ is $O(M^2)$ because the matrix \mathbf{B}_M^{-1} is pre-computed and stored.

The approximation accuracy depends critically on both the interpolating subspace W_M^g and the interpolation point set T_M . In what follows, we review the original empirical interpolation and introduce a first-order empirical interpolation for constructing W_M^g and T_M .

2.2. Empirical interpolation method

The empirical interpolation method was first proposed in [39] to enable efficient RB approximation of PDEs with nonaffine parameter dependence and subsequently extended to nonlinear parametrized PDEs [34]. We follow the empirical interpolation procedure described in [60] to construct W_M^g and T_M . We assume that we are given a sample set $S_N = \{\boldsymbol{\mu}_1 \in \mathcal{D}, \dots, \boldsymbol{\mu}_N \in \mathcal{D}\}$. We then introduce two separate RB spaces

$$W_N^u = \text{span}\{\zeta_n(\mathbf{x}) \equiv u(\mathbf{x}, \boldsymbol{\mu}_n), 1 \leq n \leq N\}, \quad (5a)$$

$$W_N^g = \text{span}\{\xi_n(\mathbf{x}) \equiv g(\zeta_n(\mathbf{x}), \boldsymbol{\mu}_n), 1 \leq n \leq N\}. \quad (5b)$$

We assume that the dimension of these two RB spaces is equal to N . First, we find

$$j_1 = \arg \max_{1 \leq j \leq N} \|\xi_j\|_{L^\infty(\Omega)}, \quad (6)$$

and set

$$\widehat{\mathbf{x}}_1 = \arg \sup_{\mathbf{x} \in \Omega} |\xi_{j_1}(\mathbf{x})|, \quad \psi_1(\mathbf{x}) = \xi_{j_1}(\mathbf{x}) / \xi_{j_1}(\widehat{\mathbf{x}}_1). \quad (7)$$

Then for $M = 2, \dots, N$, we solve the linear systems

$$\sum_{m=1}^{M-1} \psi_m(\widehat{\mathbf{x}}_k) \sigma_{nm} = \xi_n(\widehat{\mathbf{x}}_k), \quad 1 \leq k \leq M-1, \quad (8)$$

for $n = 1, \dots, N$; we find

$$j_M = \arg \max_{1 \leq n \leq N} \left\| \xi_n(\mathbf{x}) - \sum_{m=1}^{M-1} \sigma_{nm} \psi_m(\mathbf{x}) \right\|_{L^\infty(\Omega)}, \quad (9)$$

and set

$$\widehat{\mathbf{x}}_M = \arg \sup_{\mathbf{x} \in \Omega} |r_M(\mathbf{x})|, \quad \psi_M(\mathbf{x}) = r_M(\mathbf{x}) / r_M(\widehat{\mathbf{x}}_M), \quad (10)$$

where the residual function $r_M(\mathbf{x})$ is given by

$$r_M(\mathbf{x}) = \xi_{j_M}(\mathbf{x}) - \sum_{m=1}^{M-1} \sigma_{j_M m} \psi_m(\mathbf{x}). \quad (11)$$

In essence, the interpolation point $\hat{\mathbf{x}}_M$ and the basis function $\psi_M(\mathbf{x})$ are the maximum point and the normalization of the residual function $r_M(\mathbf{x})$ which results from the interpolation of $\xi_{j_M}(\mathbf{x})$ by using the previous interpolation point set T_{M-1} and basis set W_{M-1}^g . Note that the ordering of the snapshot functions in the space W_N^g does not affect the interpolation points and basis functions. In other words, the EIM yields exactly the same interpolation points and basis functions regardless of the ordering of the functions in W_M^g .

The EIM procedure constructs nested sets of interpolation points $T_M, 1 \leq M \leq N$, and nested subspaces $W_M^g = \text{span}\{\psi_m, 1 \leq m \leq M\}, 1 \leq M \leq N$. It is shown in [60] this construction of the interpolation points and the basis functions is well-defined, meaning that the basis functions are linearly independent and, in particular, the matrix $B_{M,km} = \psi_m(\hat{\mathbf{x}}_k)$ is invertible. Furthermore, the interpolation is exact for all ξ in W_M^g .

For any given sample set S_N , the number of interpolation points in T_M and basis functions in W_M^g can not exceed N . The choice of the sample set S_N may have a crucial impact on the performance of the method. In order to achieve a desired accuracy, one may need to choose the sample set S_N conservatively large enough. In the context of the reduced basis approach for parametrized PDEs, a large sample set S_N will incur a high computational cost for the offline stage because we must compute N solutions of the FOM to construct the function spaces defined in (5). Therefore, it is desirable to keep S_N as small as possible, while being able to achieve the desired accuracy. For nonlinear elliptic PDEs considered herein as well as other nonlinear parametrized PDEs considered elsewhere [20, 34, 40, 41, 42, 43, 44], the computational complexity of ROMs via empirical interpolation during the online stage is $O(MN^2 + N^3)$ per Newton iteration. While the online cost scales cubically with N , it scales linearly with M . Therefore, we usually use $M > N$ to make the approximation of the nonlinear terms highly accurate, thereby obtaining stable and accurate ROMs. This can only happen if we use a larger sample set $S_M = \{\boldsymbol{\mu}_1 \in \mathcal{D}, \dots, \boldsymbol{\mu}_M \in \mathcal{D}\}$ so that $S_N \subset S_M$ to construct the function space $W_M^g = \text{span}\{\xi_m(\mathbf{x}) \equiv g(u(\mathbf{x}, \boldsymbol{\mu}_m), \boldsymbol{\mu}_m), 1 \leq m \leq M\}$, which requires M solutions of the FOM in the offline stage.

2.3. First-order empirical interpolation method

The main idea of the first-order empirical interpolation method is based on the first-order Taylor expansion

$$g_n^{(1)}(u, \boldsymbol{\mu}) = g(\zeta_n, \boldsymbol{\mu}_n) + \frac{\partial g(\zeta_n, \boldsymbol{\mu}_n)}{\partial u}(u - \zeta_n) + \frac{\partial g(\zeta_n, \boldsymbol{\mu}_n)}{\partial \boldsymbol{\mu}} \cdot (\boldsymbol{\mu} - \boldsymbol{\mu}_n) \quad (12)$$

for $1 \leq n \leq N$. Each $g_n^{(1)}(u, \boldsymbol{\mu})$ is a first-order approximation to $g(u, \boldsymbol{\mu})$ at $(\zeta_n, \boldsymbol{\mu}_n)$. As $g(\zeta_n, \boldsymbol{\mu}_n)$ is a zero-order approximation to $g(u, \boldsymbol{\mu})$, the original empirical interpolation method only uses zero-order approximations to construct the interpolation points and interpolating functions. In order to improve the method, we use the first-order partial derivatives to construct additional interpolation points and basis functions as follows.

In addition to W_N^u and W_N^g defined in (5), we require $\frac{\partial g(\zeta_n, \boldsymbol{\mu}_n)}{\partial u}$ and $\frac{\partial g(\zeta_n, \boldsymbol{\mu}_n)}{\partial \boldsymbol{\mu}}$ for $1 \leq n \leq N$. These partial derivatives are inexpensive to compute if $\zeta_n, 1 \leq n \leq N$, are already computed. In the context of this paper, the ζ_n are numerical solutions of the parametrized PDEs at the parameter points in the sample set S_N , which can be computationally expensive. Once the ζ_n are computed, evaluating the partial derivatives of g can have a similar cost as evaluating g itself. We then introduce

$$\vartheta_{(n-1)N+k}(\boldsymbol{x}) = \frac{\partial g(\zeta_n(\boldsymbol{x}), \boldsymbol{\mu}_n)}{\partial u}(\zeta_k(\boldsymbol{x}) - \zeta_n(\boldsymbol{x})), \quad (13)$$

and

$$\vartheta_{N^2+(n-1)N+k}(\boldsymbol{x}) = \frac{\partial g(\zeta_n(\boldsymbol{x}), \boldsymbol{\mu}_n)}{\partial \boldsymbol{\mu}} \cdot (\boldsymbol{\mu}_k - \boldsymbol{\mu}_n), \quad (14)$$

for $1 \leq k, n \leq N$. Although there are $2N^2$ functions $\vartheta_n(\boldsymbol{x}), 1 \leq n \leq 2N^2$, they are not linearly independent because there are $2N$ zero functions in (13) and (14) corresponding to $k = n$. As a result, there are at most $2(N^2 - N)$ non-zero functions. Furthermore, if g does not explicitly depend on $\boldsymbol{\mu}$ then the functions in (14) are zero because we have $\frac{\partial g(\zeta_n, \boldsymbol{\mu}_n)}{\partial \boldsymbol{\mu}} = 0$. In this case, there are at most $N^2 - N$ non-zero functions. Let K be the number of linearly independent non-zero functions in the set $\{\vartheta_n(\boldsymbol{x}), 1 \leq n \leq 2N^2\}$. Without loss of generality, we denote those linearly independent functions as $\varrho_k(\boldsymbol{x}), 1 \leq k \leq K$, and introduce the the following function space

$$W_K^{\partial g} = \text{span}\{\varrho_k(\boldsymbol{x}), 1 \leq k \leq K\}. \quad (15)$$

The dimension of this function space will depend on the functional form of the nonlinear function g .

We pursue two different FOEIM algorithms to construct the basis functions and interpolation points. For the FOEIM Algorithm I, the first N interpolation points and basis functions are obtained by using the empirical interpolation procedure described in the previous subsection. The additional interpolation points and basis functions are calculated as follows. For $M = N + 1, \dots, N + K$, we solve the linear systems

$$\sum_{m=1}^{M-1} \psi_m(\hat{\mathbf{x}}_k) \sigma_{nm} = \varrho_n(\hat{\mathbf{x}}_k), \quad 1 \leq k \leq M-1, \quad (16)$$

for $n = 1, \dots, K$; we find

$$j_M = \arg \max_{1 \leq n \leq K} \left\| \varrho_n(\mathbf{x}) - \sum_{m=1}^{M-1} \sigma_{nm} \psi_m(\mathbf{x}) \right\|_{L^\infty(\Omega)}, \quad (17)$$

and set

$$\hat{\mathbf{x}}_M = \arg \sup_{\mathbf{x} \in \Omega} |r_M(\mathbf{x})|, \quad \psi_M(\mathbf{x}) = r_M(\mathbf{x})/r_M(\hat{\mathbf{x}}_M), \quad (18)$$

where the residual function $r_M(\mathbf{x})$ is given by

$$r_M(\mathbf{x}) = \varrho_{j_M}(\mathbf{x}) - \sum_{m=1}^{M-1} \sigma_{j_M m} \psi_m(\mathbf{x}). \quad (19)$$

The FOEIM Algorithm I constructs the first N interpolation points and basis functions by applying the EIM to the Lagrange space W_N^g , and the next K interpolation points and basis functions by applying the EIM to the Taylor space $W_K^{\partial g}$. Hence, the FOEIM Algorithm I includes partial derivative information only when $M > N$.

For the FOEIM Algorithm II, we combine the Lagrange space W_N^g and the Taylor space $W_K^{\partial g}$ into the following Lagrange-Taylor space

$$W_L^{\text{LT}g} = W_N^g \oplus W_K^{\partial g} \equiv \text{span}\{\varsigma_1, \dots, \varsigma_L\}, \quad (20)$$

where $L = N + K$ is the dimension of the Lagrange-Taylor space $W_L^{\text{LT}g}$. We then apply the EIM described in the previous subsection to $W_L^{\text{LT}g}$ to obtain L interpolation points and basis functions. First, we find

$$j_1 = \arg \max_{1 \leq j \leq L} \|\varsigma_j\|_{L^\infty(\Omega)}, \quad (21)$$

and set

$$\widehat{\mathbf{x}}_1 = \arg \sup_{\mathbf{x} \in \Omega} |\varsigma_{j_1}(\mathbf{x})|, \quad \psi_1(\mathbf{x}) = \varsigma_{j_1}(\mathbf{x}) / \varsigma_{j_1}(\widehat{\mathbf{x}}_1). \quad (22)$$

For $M = 2, \dots, L$, we solve the linear systems

$$\sum_{m=1}^{M-1} \psi_m(\widehat{\mathbf{x}}_k) \sigma_{lm} = \varsigma_l(\widehat{\mathbf{x}}_k), \quad 1 \leq k \leq M-1, 1 \leq l \leq L, \quad (23)$$

we then find

$$j_M = \arg \max_{1 \leq l \leq L} \left\| \varsigma_l(\mathbf{x}) - \sum_{m=1}^{M-1} \sigma_{lm} \psi_m(\mathbf{x}) \right\|_{L^\infty(\Omega)}, \quad (24)$$

and set

$$\widehat{\mathbf{x}}_M = \arg \sup_{\mathbf{x} \in \Omega} |r_M(\mathbf{x})|, \quad \psi_M(\mathbf{x}) = r_M(\mathbf{x}) / r_M(\widehat{\mathbf{x}}_M), \quad (25)$$

where the residual function $r_M(\mathbf{x})$ is given by

$$r_M(\mathbf{x}) = \varsigma_{j_M}(\mathbf{x}) - \sum_{m=1}^{M-1} \sigma_{j_M m} \psi_m(\mathbf{x}). \quad (26)$$

Note that the interpolation points and basis functions generated by the FOEIM Algorithm II are independent of the ordering of the functions in the space W_L^{LTg} . Therefore, unlike the FOEIM Algorithm I, the FOEIM Algorithm II includes partial derivative information even when $M < N$.

For any given parameter sample set S_N , the two FOEIM algorithms construct nested sets of interpolation points $T_M = \{\widehat{\mathbf{x}}_m\}_{m=1}^M$, $1 \leq M \leq L$, and nested subspaces $W_M^g = \text{span}\{\psi_m, 1 \leq m \leq M\}$, $1 \leq M \leq L$. Although the same notations are used to label the interpolation points and basis functions constructed using the EIM and FOEIM algorithms, each algorithm generate different sets of interpolation points and basis functions. We point out the fact that the interpolation points and basis functions of the EIM are a subset of those of the FOEIM Algorithm I. However, this is not the case for the FOEIM Algorithm II. Indeed, the first N interpolation points and basis functions of the FOEIM Algorithm II can be different from those of the EIM. For the same sample set S_N , the FOEIM algorithms improve the EIM by leveraging the first-order partial derivatives to generate interpolation points and basis functions.

The FOEIM algorithms have all the desirable properties of the EIM. The algorithms are well-defined in the sense that the basis functions are linearly independent and the matrix \mathbf{B}_M with entries $B_{M,ij} = \psi_j(\hat{\mathbf{x}}_i)$, $1 \leq i, j, \leq M$, is invertible. We follow [60] to show an intermediate result:

Lemma 1. *Assume that $W_{M-1}^g = \text{span}\{\psi_1, \dots, \psi_{M-1}\}$ is of dimension $M-1$ and that \mathbf{B}_{M-1} is invertible, then we have $v_{M-1} = v$ for any $v \in W_{M-1}^g$, where v_{M-1} is the interpolant of v as given below*

$$v_{M-1} = \sum_{j=1}^{M-1} \beta_{M-1,j} \psi_j, \quad (27)$$

where the $\beta_{M-1,j}$ is the solution of

$$\sum_{j=1}^{M-1} \psi_j(\hat{\mathbf{x}}_i) \beta_{M-1,j} = v(\hat{\mathbf{x}}_i), \quad i = 1, \dots, M-1. \quad (28)$$

In other words, the interpolation is exact for all v in W_{M-1}^g .

Proof. For $v \in W_{M-1}^g$, which can be expressed as $v(\mathbf{x}) = \sum_{m=1}^{M-1} \gamma_{M-1,m} \psi_m(\mathbf{x})$, we consider $\mathbf{x} = \hat{\mathbf{x}}_m$, $1 \leq m \leq M-1$, to arrive at $v(\hat{\mathbf{x}}_m) = \sum_{j=1}^{M-1} \gamma_{M-1,j} \psi_j(\hat{\mathbf{x}}_m)$, $1 \leq m \leq M-1$. It thus follows from the invertibility of \mathbf{B}_{M-1} that $\boldsymbol{\beta}_{M-1} = \boldsymbol{\gamma}_{M-1}$; and hence $v_{M-1} = v$. \square

We thus obtain the following theorem whose proof is given in [60]:

Theorem 1. *Assume that the dimension of the Lagrange-Taylor space $W_L^{\text{LT}g}$ is L ; then, for any $M \leq L$, the space $W_M^g = \text{span}\{\psi_1, \dots, \psi_M\}$ is of dimension M . In addition, the matrix \mathbf{B}_M is lower triangular with unity diagonal.*

Proof. We shall proceed by induction. Clearly, $W_1 = \text{span}\{\psi_1\}$ is of dimension 1 and the matrix $\mathbf{B}_1 = 1$ is invertible. Next we assume that $W_{M-1}^g = \text{span}\{\psi_1, \dots, \psi_{M-1}\}$ is of dimension $M-1$ and the matrix \mathbf{B}_{M-1} is invertible; we must then prove (i) $W_M^g = \text{span}\{\psi_1, \dots, \psi_M\}$ is of dimension M and (ii) the matrix \mathbf{B}_M is invertible. To prove (i), we note from our ‘‘arg max’’ construction (24) and the assumption stated in Theorem 1 that $\|r_M(\mathbf{x})\|_{L^\infty(\Omega)} > 0$. Hence, if $\dim(W_M^g) \neq M$, we have $\varsigma_{jM} \in W_{M-1}^g$ and thus $\|r_M(\mathbf{x})\|_{L^\infty(\Omega)} = 0$ by Lemma 1; however, the latter contradicts $\|r_M(\mathbf{x})\|_{L^\infty(\Omega)} > 0$. To prove (ii), we just note from the construction procedure (21)-(26) that $B_{M,ij} = r_j(\hat{\mathbf{x}}_i)/r_j(\hat{\mathbf{x}}_j) = 0$ for $i < j$; that $B_{M,ij} =$

$r_j(\widehat{\mathbf{x}}_i)/r_j(\widehat{\mathbf{x}}_j) = 1$ for $i = j$; and that $|B_{M,ij}| = |r_j(\widehat{\mathbf{x}}_i)/r_j(\widehat{\mathbf{x}}_j)| \leq 1$ for $i > j$ since $\widehat{\mathbf{x}}_j = \arg \max_{\mathbf{x} \in \Omega} |r_j(\mathbf{x})|$, $1 \leq j \leq M$. Hence, \mathbf{B}_M is lower triangular with unity diagonal. \square

This theorem implies that the procedure yields unique interpolation points and linearly independent basis functions as long as M is less than or equal to the dimension of the function space used to construct the basis functions and the interpolation points. Furthermore, the procedure reorders members of the function space in such a way that $W_M^g = \text{span}\{\varsigma_{j_1}, \dots, \varsigma_{j_M}\} = \text{span}\{\psi_1, \dots, \psi_M\}$. Hence, the procedure allows for selecting a subset of basis functions from a larger set. The error analysis of the interpolation procedure involves the Lebesgue constant as follows

Lemma 2. *Let $g_M(\mathbf{x}, \boldsymbol{\mu})$ defined by (1) be the interpolant of the parametrized function $g(u(\mathbf{x}, \boldsymbol{\mu}), \boldsymbol{\mu})$. The interpolation error (4) is bounded by*

$$\varepsilon_M(\boldsymbol{\mu}) \leq (1 + \Lambda_M) \inf_{v_M \in W_M^g} \|g(u(\mathbf{x}, \boldsymbol{\mu}), \boldsymbol{\mu}) - v_M\|_{L^\infty(\Omega)}, \quad (29)$$

where Λ_M is the Lebesgue constant

$$\Lambda_M = \sup_{\mathbf{x} \in \Omega} \sum_{j=1}^M \left| \sum_{m=1}^M \psi_m(\mathbf{x}) [\mathbf{B}_M]_{mj}^{-1} \right|. \quad (30)$$

The last term in the right hand side of the above inequality is known as the best approximation error. This Lemma has been proven in [39]. Furthermore, an upper-bound for the Lebesgue constant is $2^M - 1$ [60].

For nonlinear elliptic PDEs considered herein, the computational complexity of ROMs via first-order empirical interpolation during the online stage is also $O(MN^2 + N^3)$ per Newton iteration. Therefore, we can improve the accuracy of ROMs by using a larger number of interpolation points and basis functions to approximate the nonlinear terms. Unlike the EIM procedure described earlier, the FOEIM procedure requires N solutions of the FOM in the offline stage even when we choose $M > N$ owing to the derivative-based function space $W_K^{\partial g}$.

2.4. Empirical regression procedure

Empirical regression extends empirical interpolation by using more interpolation points than basis functions. Specifically, we use N basis functions

from the subspace $W_N^g = \text{span}\{\psi_1, \dots, \psi_N\}$ and M interpolation points from $T_M = \{\widehat{\mathbf{x}}_1, \dots, \widehat{\mathbf{x}}_M\}$ to define an approximation $g_{NM}(\mathbf{x}, \boldsymbol{\mu})$ to $g(u(\mathbf{x}, \boldsymbol{\mu}), \boldsymbol{\mu})$ as follows

$$g_{NM}(\mathbf{x}, \boldsymbol{\mu}) = \sum_{n=1}^N \beta_{N,n}(\boldsymbol{\mu}) \psi_n(\mathbf{x}). \quad (31)$$

Here the coefficients $\beta_{N,n}(\boldsymbol{\mu}), 1 \leq n \leq N$, are found as the solution of the following least-squares problem

$$\boldsymbol{\beta}_N(\boldsymbol{\mu}) = \arg \min_{\boldsymbol{\gamma}_N \in \mathbb{R}^N} \sum_{m=1}^M \left(\sum_{n=1}^N \psi_n(\widehat{\mathbf{x}}_m) \gamma_{N,n} - g(u(\widehat{\mathbf{x}}_m, \boldsymbol{\mu}), \boldsymbol{\mu}) \right)^2. \quad (32)$$

This least-squares problem reduces to the linear system (2) for $M = N$. In this case, $g_{NM}(\mathbf{x}, \boldsymbol{\mu})$ interpolates $g(u(\mathbf{x}, \boldsymbol{\mu}), \boldsymbol{\mu})$ exactly at the interpolation points. For $M > N$, $g_{NM}(\mathbf{x}, \boldsymbol{\mu})$ is the best fit in the 2-norm to $g(u(\mathbf{x}, \boldsymbol{\mu}), \boldsymbol{\mu})$ at the interpolation points. In this case, it is convenient to compute the coefficient vector $\boldsymbol{\beta}_N(\boldsymbol{\mu})$ as follows

$$\boldsymbol{\beta}_N(\boldsymbol{\mu}) = \mathbf{C}_{NM} \mathbf{b}_M(\boldsymbol{\mu}), \quad (33)$$

where $\mathbf{C}_{NM} = (\mathbf{B}_{NM} \mathbf{B}_{NM}^T)^{-1} \mathbf{B}_{NM}$, $\mathbf{B}_{NM} \in \mathbb{R}^{N \times M}$ has entries $B_{NM,nm} = \psi_n(\widehat{\mathbf{x}}_m)$ and $\mathbf{b}_M(\boldsymbol{\mu}) \in \mathbb{R}^M$ has entries $b_{M,m}(\boldsymbol{\mu}) = g(u(\widehat{\mathbf{x}}_m, \boldsymbol{\mu}), \boldsymbol{\mu})$. The cost of evaluating $\boldsymbol{\beta}_N(\boldsymbol{\mu})$ in (33) is $O(MN)$ since we compute and store \mathbf{C}_{NM} in the offline stage. We use the two FOEIM algorithms described earlier to generate interpolation points and basis functions for the empirical regression.

Empirical regression belongs to the class of oversampling methods like gappy POD [54, 55], missing point estimation [50, 56], Gauss-Newton with approximated tensors [10], and generalized EIM (GEIM) [57]. Empirical regression can provide more stable and accurate approximations than empirical interpolation for problems with noisy data [51]. For model reduction of non-linear elliptic PDEs discussed in the next section, the online complexity of ROMs via empirical regression is also $O(MN^2 + N^3)$ per Newton iteration.

2.5. A Gaussian parametrized function

We consider a parameter-dependent function $u(\mathbf{x}, \boldsymbol{\mu}) = \frac{1}{\sqrt{(x_1 - \mu_1)^2 + (x_2 - \mu_2)^2}}$ and a Gaussian parameterized function $g(u, \boldsymbol{\mu}) = \exp(-0.01u^2)$ for $\mathbf{x} \in \Omega \equiv (0, 1)^2$ and $\boldsymbol{\mu} \in \mathcal{D} \equiv [-1, -0.01]^2$. This example is modified from the one in [34]. Note that the partial derivatives $\partial g(u, \boldsymbol{\mu}) / \partial \boldsymbol{\mu}$ are zero for this particular

function. We choose for $S_{N_{\max}}$ a deterministic grid of $N_{\max} = 8 \times 8$ parameter points over \mathcal{D} , and generate a sequence of nested sample sets $S_N \in S_{N_{\max}}$ for $N = 2 \times 2, 3 \times 3, \dots, 8 \times 8$ by using the following logarithm distribution

$$y(x) = a + (b - a)(1 - \exp(-\alpha(x - a)/(b - a)))/(1 - \exp(-\alpha)), \quad (34)$$

for $x \in [a, b]$, where $a = -1, b = -0.01, \alpha = 3$. The function $y(x)$ maps a uniform grid into a logarithmic grid such that the resulting grid is clustered toward b . As shown in Figure 1, the parameter points in $S_{N_{\max}}$ are mainly distributed around the corner $(-0.01, -0.01)$ of the parameter domain.

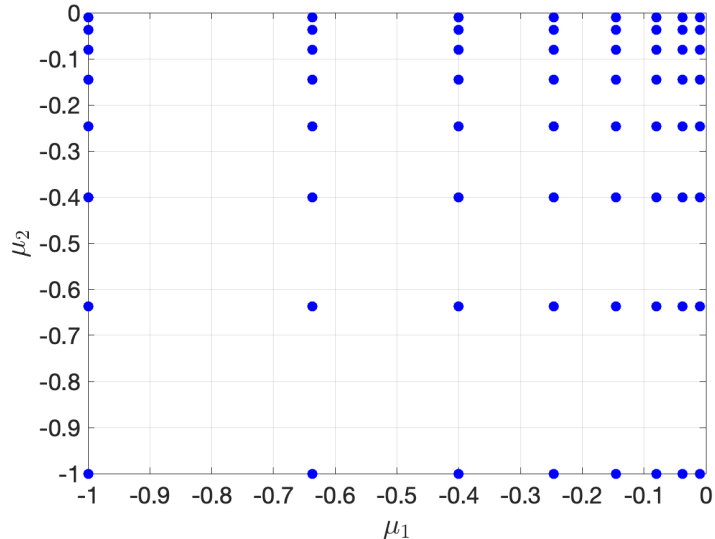


Figure 1: Parameter sample set $S_{N_{\max}}$ for the Gaussian parametrized function.

For the results reported herein, FOEIM-I and FOEIM-II refer to FOEIM Algorithm I and FOEIM Algorithm II, respectively. Furthermore, FOERM-I (respectively, FOERM-II) refers to empirical regression which uses the interpolation points and the basis functions computed by FOEIM-I (respectively, FOEIM-II). We consider three different values of M , namely, $M = N, M = 2N$, and $M = 3N$, for those methods. The interpolation points are plotted in Figure 2 for $M = 2N = 128$. We note that the interpolation points are largely allocated around the origin $(0, 0)$ of the physical domain Ω . This is because $u(\mathbf{x}, \boldsymbol{\mu})$ varies most significantly at $\mathbf{x} = (0, 0)$. The two FOEIM algorithms yield similar distributions of the interpolation points in the physical domain.

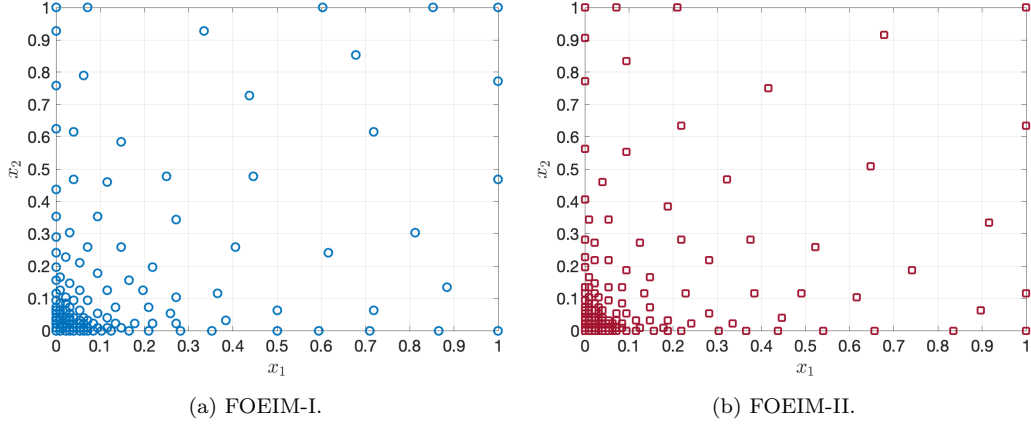
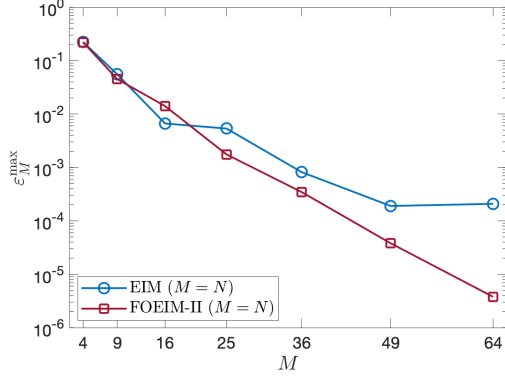


Figure 2: Distribution of interpolation points in the physical domain for FOEIM-I and FOEIM-II for $M = 2N = 128$.

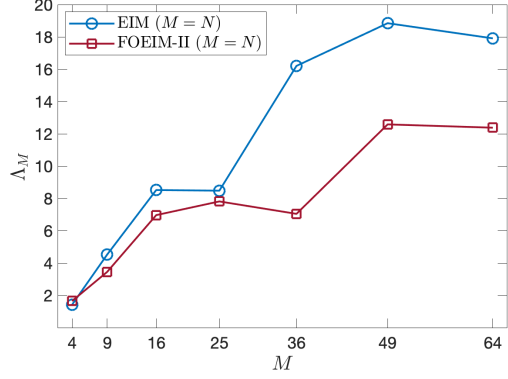
We now introduce a uniform grid of size $N_{\text{Test}} = 30 \times 30$ as a parameter test sample S_{Test}^g , and define

$$\varepsilon_M^{\max} = \max_{\boldsymbol{\mu} \in S_{\text{Test}}^g} \|g(u(\boldsymbol{x}, \boldsymbol{\mu}), \boldsymbol{\mu}) - g_M(\boldsymbol{x}, \boldsymbol{\mu})\|_{L^\infty(\Omega)} \quad (35)$$

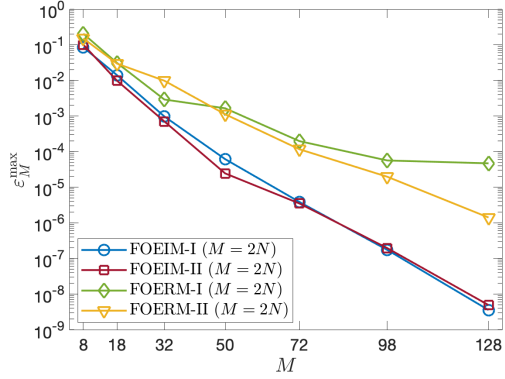
as the maximum interpolation error. We display in Figure 3 ε_M^{\max} and Λ_M as a function of M . We observe that ε_M^{\max} converge rapidly with M while the Lebesgue constant grows slowly with M . These results are expected: although $g(u, \boldsymbol{\mu})$ varies rapidly as $\boldsymbol{\mu}$ approaches 0 and \boldsymbol{x} approaches 0, $g(u, \boldsymbol{\mu})$ is nevertheless quite smooth in the prescribed parameter domain \mathcal{D} . We see from Figure 3(a) that FOEIM-II yields considerably smaller errors than EIM for $M = N = 64$, which can be attributed to the use of partial derivatives. We also observe from Figure 3(c)-(e) that FOEIM-I and FOEIM-II yield similar errors for $M = 2N$ and $M = 3N$, while FOERM-II tends to yield smaller errors than FOERM-I. These results are also shown in Table 1 and Table 2. We see from Table 1 that increasing $M = N$ to $M = 2N$ and $M = 3N$ reduces the maximum interpolation error by several orders of magnitudes for FOEIM-I and FOEIM-II. We observe from Table 2 that the maximum regression error drops slightly as we increase $M = N$ to $M = 2N$ for FOERM-I and FOERM-II. However, increasing $M = 2N$ to $M = 3N$ does not really improve the regression error. These results imply that empirical interpolation performs better than empirical regression for the same number of interpolation points.



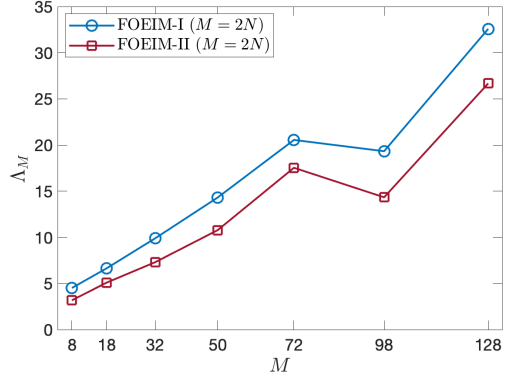
(a) Maximum interpolation error.



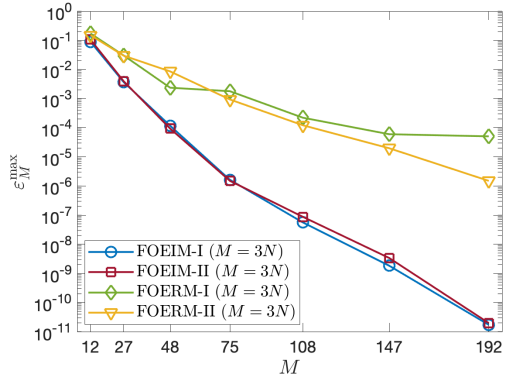
(b) Lebesgue constant.



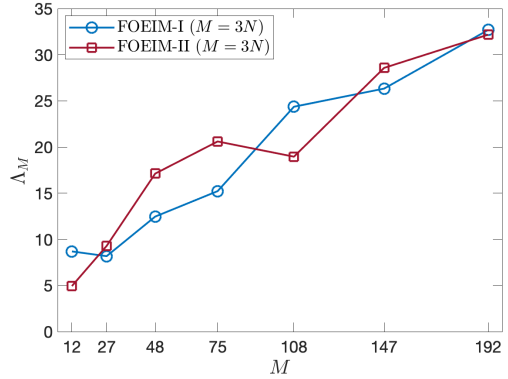
(c) Maximum interpolation error.



(d) Lebesgue constant.



(e) Maximum interpolation error.



(f) Lebesgue constant.

Figure 3: Convergence of the maximum interpolation error and the Lebesgue constant as a function of M for EIM, FOEIM-I, FOEIM-II, FOERM-I, FOERM-II.

N	FOEIM-I $M = N$	FOEIM-I $M = 2N$	FOEIM-I $M = 3N$	FOEIM-II $M = N$	FOEIM-II $M = 2N$	FOEIM-II $M = 3N$
4	2.24e-1	8.50e-2	8.90e-2	2.21e-1	1.01e-1	1.06e-1
9	5.55e-2	1.40e-2	3.69e-3	4.51e-2	9.79e-3	3.95e-3
16	6.65e-3	9.73e-4	1.17e-4	1.41e-2	7.05e-4	9.34e-5
25	5.34e-3	6.16e-5	1.63e-6	1.75e-3	2.45e-5	1.51e-6
36	8.16e-4	3.86e-6	5.60e-8	3.45e-4	3.50e-6	8.73e-8
49	1.90e-4	1.74e-7	1.84e-9	3.81e-5	1.95e-7	3.38e-9
64	2.08e-4	3.56e-9	1.72e-11	3.77e-6	4.91e-9	1.97e-11

Table 1: Maximum interpolation error ε_M^{\max} as a function of N and M for FOEIM-I and FOEIM-II. Note that FOEIM-I is the same as EIM for $M = N$.

N	FOERM-I $M = N$	FOERM-I $M = 2N$	FOERM-I $M = 3N$	FOERM-II $M = N$	FOERM-II $M = 2N$	FOERM-II $M = 3N$
4	2.24e-1	2.05e-1	1.72e-1	2.21e-1	1.51e-1	1.50e-1
9	5.55e-2	3.09e-2	3.02e-2	4.51e-2	2.96e-2	2.98e-2
16	6.65e-3	2.91e-3	2.37e-3	1.41e-2	9.81e-3	8.58e-3
25	5.34e-3	1.65e-3	1.80e-3	1.75e-3	1.12e-3	9.34e-4
36	8.16e-4	1.97e-4	2.21e-4	3.45e-4	1.17e-4	1.22e-4
49	1.90e-4	5.65e-5	6.00e-5	3.81e-5	1.97e-5	1.98e-5
64	2.08e-4	4.69e-5	5.07e-5	3.77e-6	1.41e-6	1.50e-6

Table 2: Maximum regression error ε_M^{\max} as a function of N and M for FOERM-I and FOERM-II. Note that FOERM-I is the same as EIM for $M = N$.

3. Nonlinear elliptic equations

3.1. A model problem

We consider the following parametrized nonlinear elliptic PDE

$$-\nabla^2 u + \mu_1 \exp(\sin(\mu_2 u)) = 100 \sin(2\pi x_1) \cos(2\pi x_2), \quad \text{in } \Omega, \quad (36)$$

with homogeneous Dirichlet condition on the boundary $\partial\Omega$, where $\Omega = (0, 1)^2$ and $\boldsymbol{\mu} \in \mathcal{D} \equiv [1, 10]^2$. The output of interest is the average of the field variable over the physical domain. The weak formulation is then stated as: given $\boldsymbol{\mu} \in \mathcal{D}$, find $s(\boldsymbol{\mu}) = \int_{\Omega} u(\boldsymbol{\mu})$, where $u(\boldsymbol{\mu}) \in X \subset H_0^1(\Omega) \equiv \{v \in H^1(\Omega) \mid v|_{\partial\Omega} = 0\}$ is the solution of

$$a(u(\boldsymbol{\mu}), v) + \mu_1 \int_{\Omega} g(u(\boldsymbol{\mu}), \boldsymbol{\mu}) v = f(v), \quad \forall v \in X, \quad (37)$$

where

$$a(w, v) = \int_{\Omega} \nabla w \cdot \nabla v, \quad f(v) = 100 \int_{\Omega} \sin(2\pi x_1) \cos(2\pi x_2) v, \quad (38)$$

and

$$g(u(\boldsymbol{\mu}), \boldsymbol{\mu}) = \exp(\sin(\mu_2 u(\boldsymbol{\mu}))). \quad (39)$$

The finite element (FE) approximation space is $X = \{v \in H_0^1(\Omega) : v|_K \in \mathcal{P}^3(T), \forall T \in \mathcal{T}_h\}$, where $\mathcal{P}^3(T)$ is a space of polynomials of degree 3 on an element $T \in \mathcal{T}_h$ and \mathcal{T}_h is a finite element grid of 32×32 quadrilaterals. The dimension of the FE space is $\mathcal{N} = 9409$.

3.2. Reduced basis approximation

We introduce the parameter sample set $S_N = \{\boldsymbol{\mu}_1 \in \mathcal{D}, \dots, \boldsymbol{\mu}_N \in \mathcal{D}\}$, and associated RB space $W_N^u = \text{span}\{\zeta_j \equiv u(\boldsymbol{\mu}_j), 1 \leq j \leq N\}$, where $u(\boldsymbol{\mu}_j)$ is the solution of (37) for $\boldsymbol{\mu} = \boldsymbol{\mu}_j$. We then orthonormalize the $\zeta_j, 1 \leq j \leq N$, with respect to $(\cdot, \cdot)_X$ so that $(\zeta_i, \zeta_j)_X = \delta_{ij}, 1 \leq i, j \leq N$. The RB approximation is obtained by a standard Galerkin projection: given $\boldsymbol{\mu} \in \mathcal{D}$, we evaluate $s_N(\boldsymbol{\mu}) = \int_{\Omega} u_N(\boldsymbol{\mu})$, where $u_N(\boldsymbol{\mu}) \in W_N^u$ is the solution of

$$a(u_N(\boldsymbol{\mu}), v) + \mu_1 \int_{\Omega} g(u_N(\boldsymbol{\mu}), \boldsymbol{\mu}) v = f(v), \quad \forall v \in W_N^u. \quad (40)$$

We now express $u_N(\boldsymbol{\mu}) = \sum_{n=1}^N \alpha_{N,n}(\boldsymbol{\mu}) \zeta_n$ and choose test functions $v = \zeta_j, 1 \leq j \leq N$, in (40), we obtain the nonlinear algebraic system

$$\mathbf{A}_N \boldsymbol{\alpha}_N(\boldsymbol{\mu}) + \mu_1 \mathbf{G}_N(\boldsymbol{\alpha}_N(\boldsymbol{\mu}), \boldsymbol{\mu}) = \mathbf{F}_N \quad (41)$$

where, for $1 \leq n, j \leq N$, we have

$$A_{N,jn} = a(\zeta_j, \zeta_n), \quad F_{N,j} = f(\zeta_j), \quad (42)$$

and

$$G_{N,j}(\boldsymbol{\alpha}_N(\boldsymbol{\mu}), \boldsymbol{\mu}) = \int_{\Omega} g(u_N(\boldsymbol{\mu}), \boldsymbol{\mu}) \zeta_j. \quad (43)$$

Both \mathbf{A}_N and \mathbf{F}_N can be pre-computed in the offline stage owing to their parameter independence, whereas \mathbf{G}_N can not be pre-computed due to the nonlinearity of the function g .

We use Newton method to linearize (41) at a current iterate $\bar{\alpha}_N(\boldsymbol{\mu})$ to arrive at the following linear system

$$(\mathbf{A}_N + \mu_1 \mathbf{D}_N(\bar{\alpha}_N(\boldsymbol{\mu}), \boldsymbol{\mu})) \delta \alpha_N(\boldsymbol{\mu}) = \mathbf{F}_N - \mathbf{A}_N \bar{\alpha}_N(\boldsymbol{\mu}) - \mu_1 \mathbf{G}_N(\bar{\alpha}_N(\boldsymbol{\mu}), \boldsymbol{\mu}) \quad (44)$$

where, for $1 \leq n, j \leq N$, we have

$$D_{N,jn}(\bar{\alpha}_N(\boldsymbol{\mu}), \boldsymbol{\mu}) = \int_{\Omega} g'_u(\bar{u}_N(\boldsymbol{\mu}), \boldsymbol{\mu}) \zeta_n \zeta_j. \quad (45)$$

Here g'_u is the partial derivative of g with respect to the first argument. Unfortunately, the matrix \mathbf{D}_N can not be pre-computed in the offline stage due to its dependency on $g'_u(\bar{u}_N(\boldsymbol{\mu}), \boldsymbol{\mu})$. Consequently, although the linear system (44) is small, it is computationally expensive due to the \mathcal{N} -dependent complexity of forming both \mathbf{G}_N and \mathbf{D}_N . As a result, the RB approximation does not offer a significant speedup over the FE approximation.

3.3. Reduced basis approximation via empirical interpolation

To recover online \mathcal{N} -independence, we simply replace $g(u_N(\boldsymbol{\mu}), \boldsymbol{\mu})$ in (40) with the approximation $g_M(\mathbf{x}, \boldsymbol{\mu}) = \sum_{m=1}^M \beta_{M,m}(\boldsymbol{\mu}) \psi_m(\mathbf{x})$ based upon the empirical interpolation approach. This requires us to pre-compute the interpolation point set $T_M = \{\hat{\mathbf{x}}_m\}_{m=1}^M$ and the interpolating basis set $W_M^g = \text{span}\{\psi_m(\mathbf{x}), 1 \leq m \leq M\}$ for the nonlinear parametrized function $g(u(\boldsymbol{\mu}), \boldsymbol{\mu})$ in the offline stage. For the original EIM described in Section 2.2, we use the sample set S_N and the basis set W_N^u to construct T_M and W_M^g . In this case, M can not exceed N . For the first-order EIM described in Section 2.3, we need to construct the Taylor space $W_K^{\partial g}$ in (15) using S_N, W_N^u and first-order partial derivatives of $g(\zeta, \boldsymbol{\mu})$ for $(\zeta, \boldsymbol{\mu}) = (\zeta_n, \boldsymbol{\mu}_n), 1 \leq n \leq N$. Henceforth, M can be chosen many times greater than N .

In practice, the empirical interpolation is carried out over a set of discretization points on the physical domain Ω . There are two different options for the choice of the discretization points: (i) nodal points on all elements in the mesh and (ii) quadrature points on all elements in the mesh. We observe through numerical experiments that the quadrature points yield more accurate approximation than the nodal points. Hence, the interpolation points are selected from the set of quadrature points on elements in the mesh. We are going to describe the RB approximation via empirical interpolation, which turns out to be exactly the same procedure for both the original EIM and the first-order EIM.

In the online stage, our RB approximation via empirical interpolation is stated as: Given $\boldsymbol{\mu} \in \mathcal{D}$, we evaluate $s_{N,M}(\boldsymbol{\mu}) = \int_{\Omega} u_{N,M}(\boldsymbol{\mu})$, where $u_{N,M}(\boldsymbol{\mu}) \in W_N^u$ is the solution of

$$a(u_{N,M}(\boldsymbol{\mu}), v) + \mu_1 \sum_{m=1}^M \beta_{M,m}(\boldsymbol{\mu}) \int_{\Omega} \psi_m v = f(v), \quad \forall v \in W_N^u, \quad (46)$$

where the coefficients $\beta_{M,m}(\boldsymbol{\mu})$ are computed from the following linear system

$$\sum_{m=1}^M \psi_m(\widehat{\boldsymbol{x}}_k) \beta_{M,m}(\boldsymbol{\mu}) = g(u_{N,M}(\widehat{\boldsymbol{x}}_k, \boldsymbol{\mu}), \boldsymbol{\mu}), \quad 1 \leq k \leq M. \quad (47)$$

We now express $u_{N,M}(\boldsymbol{\mu}) = \sum_{n=1}^N \alpha_{N,M,n}(\boldsymbol{\mu}) \zeta_n$ and choose test functions $v = \zeta_j$, $1 \leq j \leq N$, in (46), we obtain the nonlinear algebraic system

$$\mathbf{A}_N \boldsymbol{\alpha}_{N,M}(\boldsymbol{\mu}) + \mu_1 \mathbf{E}_{N,M} \mathbf{g}_M(\boldsymbol{\alpha}_{N,M}(\boldsymbol{\mu}), \boldsymbol{\mu}) = \mathbf{F}_N, \quad (48)$$

where $\mathbf{E}_{N,M} = \mathbf{C}_{N,M} \mathbf{B}_M^{-1}$, for $1 \leq j \leq N$ and $1 \leq m, k \leq M$, we have

$$C_{N,M,jm} = \int_{\Omega} \psi_m \zeta_j, \quad B_{M,km} = \psi_m(\widehat{\boldsymbol{x}}_k), \quad (49)$$

and

$$g_{M,k}(\boldsymbol{\alpha}_{N,M}(\boldsymbol{\mu}), \boldsymbol{\mu}) = g \left(\sum_{n=1}^N \alpha_{N,M,n}(\boldsymbol{\mu}) \zeta_n(\widehat{\boldsymbol{x}}_k), \boldsymbol{\mu} \right). \quad (50)$$

The vector \mathbf{F}_N and matrices $\mathbf{A}_N, \mathbf{E}_{N,M}$ can be pre-computed in the offline stage since they are independent of $\boldsymbol{\mu}$. We form and store the Jacobian matrix of the FOM to compute \mathbf{A}_N using Jacobian-vector products during the offline stage. For large-scale problems, forming and storing the Jacobian matrix can be costly in terms of both memory storage and computational time. One possible remedy to reduce the memory storage and computational time is to use a Jacobian-free technique to compute Jacobian-vector products via finite difference. However, finite difference does not yield the exact Jacobian-vector products, a more rigorous method is to use automatic differentiation to compute the Jacobian-vector products exactly [61].

We use Newton method to linearize (48) at a given iterate $\bar{\boldsymbol{\alpha}}_{N,M}(\boldsymbol{\mu})$ to arrive at the following linear system

$$\begin{aligned} (\mathbf{A}_N + \mu_1 \mathbf{E}_{N,M} \mathbf{H}_{M,N}(\bar{\boldsymbol{\alpha}}_{N,M}(\boldsymbol{\mu}), \boldsymbol{\mu})) \delta \boldsymbol{\alpha}_N(\boldsymbol{\mu}) = \\ \mathbf{F}_N - \mathbf{A}_N \bar{\boldsymbol{\alpha}}_{N,M}(\boldsymbol{\mu}) - \mu_1 \mathbf{E}_{N,M} \mathbf{g}_M(\bar{\boldsymbol{\alpha}}_{N,M}(\boldsymbol{\mu}), \boldsymbol{\mu}) \end{aligned} \quad (51)$$

where, for $1 \leq i \leq N$ and $1 \leq k \leq M$, we have

$$H_{M,N,ki}(\bar{\alpha}_N(\boldsymbol{\mu}), \boldsymbol{\mu}) = g'_u \left(\sum_{n=1}^N \bar{\alpha}_{N,M,n}(\boldsymbol{\mu}) \zeta_n(\hat{\boldsymbol{x}}_k), \boldsymbol{\mu} \right) \zeta_i(\hat{\boldsymbol{x}}_k). \quad (52)$$

In the online stage, at each Newton iteration, we compute $\boldsymbol{g}_M(\bar{\alpha}_{N,M}(\boldsymbol{\mu}), \boldsymbol{\mu})$ from (50) and $\boldsymbol{H}_{M,N}(\bar{\alpha}_{N,M}(\boldsymbol{\mu}), \boldsymbol{\mu})$ from (52), and solve the linear system (51). The online complexity of evaluating $\boldsymbol{g}_M(\bar{\alpha}_{N,M}(\boldsymbol{\mu}), \boldsymbol{\mu})$ is $O(MN)$, while that of evaluating $\boldsymbol{H}_{M,N}(\bar{\alpha}_{N,M}(\boldsymbol{\mu}), \boldsymbol{\mu})$ is $O(MN^2)$. Hence, the overall complexity of solving the linear system (51) per Newton iteration is $O(MN^2 + N^3)$. Since $M \geq N$, the computational complexity per Newton iteration becomes $O(MN^2)$. As a result, the RB approximation via empirical interpolation can be orders of magnitude faster than the RB approximation described earlier.

It is important to note that the computational complexity scales linearly with M . Hence, it can be advantageous to increase M to improve the accuracy of the RB approximation via empirical interpolation. As M increases, we expect that the RB approximation via empirical interpolation will converge to the standard RB approximation. To assess the accuracy of the output approximation, we define the following output errors

$$\epsilon_N^s(\boldsymbol{\mu}) = |s(\boldsymbol{\mu}) - s_N(\boldsymbol{\mu})|, \quad \epsilon_{N,M}^s(\boldsymbol{\mu}) = |s(\boldsymbol{\mu}) - s_{N,M}(\boldsymbol{\mu})| \quad (53)$$

for the standard RB approximation and the RB approximation via empirical interpolation, respectively. Similarly, we introduce the following errors to assess the approximation of the solution

$$\epsilon_N^u(\boldsymbol{\mu}) = \|u(\boldsymbol{\mu}) - u_N(\boldsymbol{\mu})\|_X, \quad \epsilon_{N,M}^u(\boldsymbol{\mu}) = \|u(\boldsymbol{\mu}) - u_{N,M}(\boldsymbol{\mu})\|_X. \quad (54)$$

In general, we expect $\epsilon_{N,M}^s(\boldsymbol{\mu}) \geq \epsilon_N^s(\boldsymbol{\mu})$ and $\epsilon_{N,M}^u(\boldsymbol{\mu}) \geq \epsilon_N^u(\boldsymbol{\mu})$. The effectivities as defined below

$$\eta_{N,M}^s(\boldsymbol{\mu}) = \frac{\epsilon_{N,M}^s(\boldsymbol{\mu})}{\epsilon_N^s(\boldsymbol{\mu})}, \quad \eta_{N,M}^u(\boldsymbol{\mu}) = \frac{\epsilon_{N,M}^u(\boldsymbol{\mu})}{\epsilon_N^u(\boldsymbol{\mu})} \quad (55)$$

will measure the accuracy of the RB approximation via empirical interpolation relative to the standard RB approximation. If the effectivities are close to unity, the RB approximation via empirical interpolation can be considered as accurate as the standard RB approximation. However, if they are much greater than unity, the RB approximation via empirical interpolation will be not accurate enough.

3.4. Numerical results

We present numerical results for the model problem of Section 3.1. The first-order EIM results reported herein are obtained by using the FOEIM Algorithm I. We introduce a uniform grid of size $N_{\text{Test}} = 30 \times 30$ as a parameter test sample S_{Test}^g , and define

$$\bar{\epsilon}_N^s = \frac{\sum_{\boldsymbol{\mu} \in S_{\text{Test}}^g} \epsilon_N^s(\boldsymbol{\mu})}{\sum_{\boldsymbol{\mu} \in S_{\text{Test}}^g} |s(\boldsymbol{\mu})|}, \quad \bar{\epsilon}_N^u = \frac{\sum_{\boldsymbol{\mu} \in S_{\text{Test}}^g} \epsilon_N^u(\boldsymbol{\mu})}{\sum_{\boldsymbol{\mu} \in S_{\text{Test}}^g} \|u(\boldsymbol{\mu})\|_X}. \quad (56)$$

The quantities $\bar{\epsilon}_{N,M}^s$ and $\bar{\epsilon}_{N,M}^u$ are similarly defined via $\epsilon_{N,M}^s(\boldsymbol{\mu})$ and $\epsilon_{N,M}^u(\boldsymbol{\mu})$, respectively. We present in Figure 4 $\bar{\epsilon}_N^s$, $\bar{\epsilon}_{N,M}^s$, $\bar{\epsilon}_N^u$, and $\bar{\epsilon}_{N,M}^u$ as a function of N . As M increases, $\bar{\epsilon}_{N,M}^s$ (respectively, $\bar{\epsilon}_{N,M}^u$) converges to $\bar{\epsilon}_N^s$ (respectively, $\bar{\epsilon}_N^u$). The RB approximation based on the first-order EIM with $M = 8N$ is almost as accurate as the standard RB approximation. However, the RB approximation based on the original EIM is significantly less accurate than the standard RB approximation.

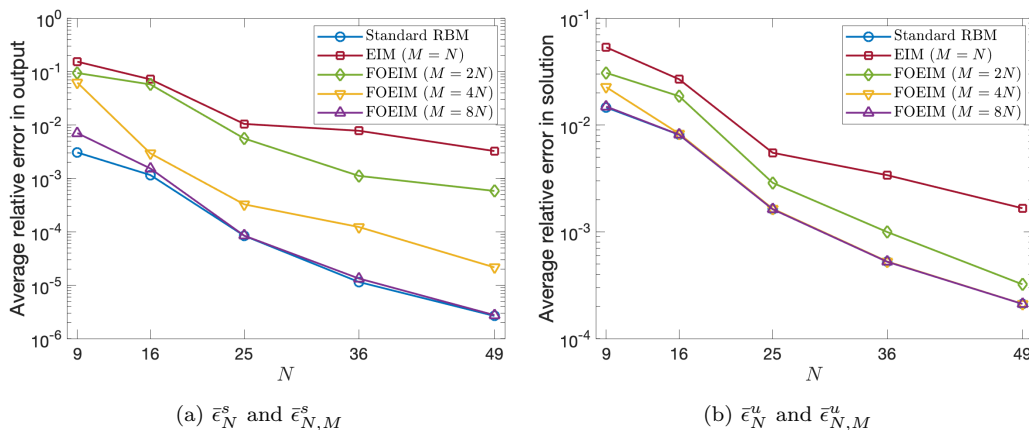


Figure 4: Convergence of the average relative error in output (a) and solution (b) for the model problem of Section 3.1.

To compare the original EIM and the first-order EIM, we introduce

$$\bar{\eta}_{N,M}^s = \frac{1}{N_{\text{Test}}} \sum_{\boldsymbol{\mu} \in S_{\text{Test}}^g} \eta_{N,M}^s(\boldsymbol{\mu}), \quad \bar{\eta}_{N,M}^u = \frac{1}{N_{\text{Test}}} \sum_{\boldsymbol{\mu} \in S_{\text{Test}}^g} \eta_{N,M}^u(\boldsymbol{\mu}). \quad (57)$$

We display in Table 3 $\bar{\eta}_{N,M}^s$ and $\bar{\eta}_{N,M}^u$ as a function of N . We observe that the average effectivities decrease toward unity as M increases. Furthermore, the

first-order EIM with $M = 8N$ yields significantly smaller output effectivities by several orders of magnitudes than the original EIM for the same dimension N . It is interesting to point out that the output effectivities are considerably larger than the solution effectivities.

N	$M = N$		$M = 2N$		$M = 4N$		$M = 8N$	
	$\bar{\eta}_{N,M}^s$	$\bar{\eta}_{N,M}^u$	$\bar{\eta}_{N,M}^s$	$\bar{\eta}_{N,M}^u$	$\bar{\eta}_{N,M}^s$	$\bar{\eta}_{N,M}^u$	$\bar{\eta}_{N,M}^s$	$\bar{\eta}_{N,M}^u$
9	193.38	4.59	102.45	2.17	26.28	1.41	5.73	1.03
16	168.25	3.03	130.03	2.07	10.81	1.04	2.34	1.00
25	396.44	3.82	224.32	2.14	12.31	1.01	2.83	1.00
36	1223.7	6.87	190.39	2.06	17.51	1.01	1.95	1.00
49	1310.14	7.67	294.96	1.52	17.92	1.00	1.98	1.00

Table 3: Average effectivities for the model problem of Section 3.1. The column with $M = N$ corresponds to the original EIM, while the columns with $M > N$ correspond to the first-order EIM.

We present in Table 4 the online computational times to calculate $s_N(\boldsymbol{\mu})$ and $s_{N,M}(\boldsymbol{\mu})$ as a function of N . The values are normalized with respect to the computational time of the truth approximation output $s(\boldsymbol{\mu})$. The computational saving is significant: for an relative accuracy of about 0.0001 ($N = 25$, $M = 200$) in the output, the reduction in online cost is more than a factor of 1000; this is mainly because the matrix assembly of the nonlinear terms for the truth approximation is computationally very expensive. The standard RB approximation has similar computational times as the truth FE approximation, and is between 100 and 1000 times slower than the RB approximation via empirical interpolation. We notice that using $M = N$ often requires more Newton iterations to converge than using $M > N$ especially when N is relatively small. As a result, the online computational time with $M = N$ is slightly higher than that $M > N$ especially for $N = 9$ and $N = 16$.

4. Nonlinear diffusion equations

4.1. A model problem

We consider a parametrized nonlinear heat conduction problem

$$-\nabla \cdot (\kappa(u, \boldsymbol{\mu}) \nabla u) = 0 \quad \text{in } \Omega, \quad (58)$$

with homogeneous boundary conditions

$$u = 0 \quad \text{on } \Gamma_D, \quad \kappa(u, \boldsymbol{\mu}) \nabla u \cdot \boldsymbol{n} = 0 \quad \text{on } \Gamma_N, \quad (59)$$

N	FEM $s(\boldsymbol{\mu})$	RBM $s_N(\boldsymbol{\mu})$	EIM $M = N$	FOEIM $M = 2N$	FOEIM $M = 4N$	FOEIM $M = 8N$
9	1	5.37e-1	1.04e-3	4.93e-4	3.31e-4	3.46e-4
16	1	5.44e-1	4.67e-4	4.59e-4	4.51e-4	5.73e-4
25	1	5.61e-1	5.17e-4	5.19e-4	5.98e-4	9.65e-4
36	1	1.51e-0	2.49e-3	3.43e-3	3.93e-3	5.00e-3
49	1	2.07e-0	3.48e-3	4.15e-3	5.09e-3	6.77e-3

Table 4: Online computational times (normalized with respect to the time to solve for $s(\boldsymbol{\mu})$) for the model problem of Section 3.1.

and non-homogeneous Neumann condition

$$\kappa(u, \boldsymbol{\mu}) \nabla u \cdot \boldsymbol{n} = \mu_1 \quad \text{on } \Gamma_Q. \quad (60)$$

Here Ω is the T -shaped domain as shown in Figure 5(a). Γ_D is the top boundary and Γ_Q is the bottom boundary, while Γ_N is the remaining part of the boundary. The parameter domain is $\mathcal{D} \equiv [1, 10] \times [0, 10]$. The thermal conductivity is a Gaussian function of the form

$$\kappa(u, \boldsymbol{\mu}) = \exp(-(u - \mu_2)^2). \quad (61)$$

The output of interest is the average of the field variable over the physical domain. For any given $\boldsymbol{\mu} \in \mathcal{D}$, we evaluate $s(\boldsymbol{\mu}) = \int_{\Omega} u(\boldsymbol{\mu})$, where $u(\boldsymbol{\mu}) \in X \subset H_0^1(\Omega) \equiv \{v \in H^1(\Omega) \mid v|_{\Gamma_D} = 0\}$ is the solution of

$$\int_{\Omega} \kappa(u(\boldsymbol{\mu}), \boldsymbol{\mu}) \nabla u \cdot \nabla v = \mu_1 \int_{\Gamma_Q} v, \quad \forall v \in X. \quad (62)$$

The FE approximation space is $X = \{v \in H_0^1(\Omega) : v|_K \in \mathcal{P}^3(T), \forall T \in \mathcal{T}_h\}$, where $\mathcal{P}^3(T)$ is a space of polynomials of degree 3 on an element $T \in \mathcal{T}_h$ and \mathcal{T}_h is a mesh of 900 quadrilaterals. The dimension of X is $\mathcal{N} = 8401$. Figure 5 shows FE solutions at two different parameter points.

4.2. Reduced basis approximation

The RB approximation is obtained by a standard Galerkin projection: given $\boldsymbol{\mu} \in \mathcal{D}$, we evaluate $s_N(\boldsymbol{\mu}) = \int_{\Omega} u_N(\boldsymbol{\mu})$, where $u_N(\boldsymbol{\mu}) \in W_N^u$ is the solution of

$$\int_{\Omega} \kappa(u_N(\boldsymbol{\mu}), \boldsymbol{\mu}) \nabla u_N \cdot \nabla v = \mu_1 \int_{\Gamma_Q} v, \quad \forall v \in W_N^u. \quad (63)$$

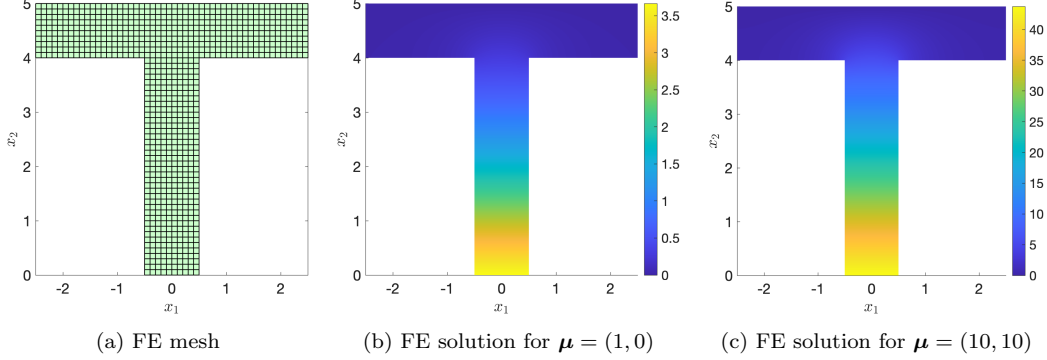


Figure 5: FE mesh and numerical solutions at two parameter points for the nonlinear heat conduction problem.

We now express $u_N(\boldsymbol{\mu}) = \sum_{n=1}^N \alpha_{N,n}(\boldsymbol{\mu}) \zeta_n$ and choose test functions $v = \zeta_j$, $1 \leq j \leq N$, in (63), we obtain the nonlinear algebraic system

$$\mathbf{A}_N(\boldsymbol{\alpha}_N(\boldsymbol{\mu}), \boldsymbol{\mu}) \boldsymbol{\alpha}_N(\boldsymbol{\mu}) = \mu_1 \mathbf{F}_N, \quad (64)$$

where, for $1 \leq n, j \leq N$, we have

$$A_{N,jn}(\boldsymbol{\alpha}_N(\boldsymbol{\mu}), \boldsymbol{\mu}) = \int_{\Omega} \kappa(u_N(\boldsymbol{\mu}), \boldsymbol{\mu}) \nabla \zeta_n \cdot \nabla \zeta_j, \quad F_{N,j} = \int_{\Gamma_Q} \zeta_j. \quad (65)$$

While \mathbf{F}_N can be pre-computed in the offline stage, \mathbf{A}_N can not be pre-computed due to the nonlinearity of the function κ . Although the nonlinear system (64) has a small number of unknowns, it is computationally expensive due to the \mathcal{N} -dependent complexity of forming \mathbf{A}_N . As a result, the RB approximation does not offer a significant speedup over the FE approximation.

4.3. Reduced basis approximation via empirical interpolation

For this particular nonlinear PDE, we apply the empirical interpolation to $\kappa(u(\boldsymbol{\mu}), \boldsymbol{\mu}) \nabla u(\boldsymbol{\mu})$, which is a vector-valued function. To this end, we introduce

$$g(u(\boldsymbol{\mu}), \boldsymbol{\mu}) = \kappa(u(\boldsymbol{\mu}), \boldsymbol{\mu}) \frac{\partial u(\boldsymbol{\mu})}{\partial x_1}, \quad h(u(\boldsymbol{\mu}), \boldsymbol{\mu}) = \kappa(u(\boldsymbol{\mu}), \boldsymbol{\mu}) \frac{\partial u(\boldsymbol{\mu})}{\partial x_2}. \quad (66)$$

The RB approximation (63) is equivalent to finding $u_N(\boldsymbol{\mu}) \in W_N^u$ such that

$$\int_{\Omega} g(u_N(\boldsymbol{\mu}), \boldsymbol{\mu}) \frac{\partial v}{\partial x_1} + \int_{\Omega} h(u_N(\boldsymbol{\mu}), \boldsymbol{\mu}) \frac{\partial v}{\partial x_2} = \mu_1 \int_{\Gamma_Q} v, \quad \forall v \in W_N^u. \quad (67)$$

Since the two nonlinear functions in (66) depends not only on the field variable but also its spatial gradient, their evaluation requires us to compute the gradient of the field variable.

To develop an efficient RB approximation, we replace the two nonlinear functions, namely $g(u_N(\boldsymbol{\mu}), \boldsymbol{\mu})$ and $h(u_N(\boldsymbol{\mu}), \boldsymbol{\mu})$, in (67) with

$$g_M(\mathbf{x}, \boldsymbol{\mu}) = \sum_{m=1}^M \beta_{M,m}(\boldsymbol{\mu}) \psi_m^g(\mathbf{x}), \quad h_M(\mathbf{x}, \boldsymbol{\mu}) = \sum_{m=1}^M \gamma_{M,m}(\boldsymbol{\mu}) \psi_m^h(\mathbf{x}) \quad (68)$$

to obtain $u_{N,M}(\boldsymbol{\mu}) \in W_N^u$ as the solution of

$$\sum_{m=1}^M \beta_{M,m}(\boldsymbol{\mu}) \int_{\Omega} \psi_m^g \frac{\partial v}{\partial x_1} + \sum_{m=1}^M \gamma_{M,m}(\boldsymbol{\mu}) \int_{\Omega} \psi_m^h \frac{\partial v}{\partial x_2} = \mu_1 \int_{\Gamma_Q} v, \quad \forall v \in W_N^u. \quad (69)$$

Here $\beta_{M,m}(\boldsymbol{\mu})$ and $\gamma_{M,m}(\boldsymbol{\mu})$ are computed from

$$\begin{aligned} \sum_{m=1}^M \psi_m^g(\widehat{\mathbf{x}}_k^g) \beta_{M,m}(\boldsymbol{\mu}) &= g(u_{N,M}(\widehat{\mathbf{x}}_k^g, \boldsymbol{\mu}), \boldsymbol{\mu}), \quad 1 \leq k \leq M, \\ \sum_{m=1}^M \psi_m^h(\widehat{\mathbf{x}}_k^h) \gamma_{M,m}(\boldsymbol{\mu}) &= h(u_{N,M}(\widehat{\mathbf{x}}_k^h, \boldsymbol{\mu}), \boldsymbol{\mu}), \quad 1 \leq k \leq M, \end{aligned} \quad (70)$$

where $T_M^g = \{\widehat{\mathbf{x}}_m^g\}_{m=1}^M$, $W_M^g = \text{span}\{\psi_m^g(\mathbf{x})\}_{m=1}^M$, and $T_M^h = \{\widehat{\mathbf{x}}_m^h\}_{m=1}^M$, $W_M^h = \text{span}\{\psi_m^h(\mathbf{x})\}_{m=1}^M$ are the interpolation point sets and basis sets for approximating $g(u_N(\boldsymbol{\mu}), \boldsymbol{\mu})$ and $h(u_N(\boldsymbol{\mu}), \boldsymbol{\mu})$, respectively. These interpolation point sets and basis sets are pre-computed in the offline stage. For the first-order EIM described in Section 2.3, we employ the partial derivatives of the nonlinear functions as follows

$$\begin{aligned} \vartheta_{(n-1)N+k}^g(\mathbf{x}) &= \frac{\partial \kappa(\zeta_n(\mathbf{x}), \boldsymbol{\mu}_n)}{\partial u} \frac{\partial \zeta_n(\boldsymbol{\mu}_n)}{\partial x_1} (\zeta_k(\mathbf{x}) - \zeta_n(\mathbf{x})) + \\ &\quad \kappa(\zeta_n(\mathbf{x}), \boldsymbol{\mu}_n) \frac{\partial (\zeta_k(\mathbf{x}) - \zeta_n(\mathbf{x}))}{\partial x_1}, \end{aligned} \quad (71)$$

and

$$\vartheta_{N^2+(n-1)N+k}^g(\mathbf{x}) = \frac{\partial \kappa(\zeta_n(\mathbf{x}), \boldsymbol{\mu}_n)}{\partial \boldsymbol{\mu}} \frac{\partial \zeta_n(\boldsymbol{\mu}_n)}{\partial x_1} \cdot (\boldsymbol{\mu}_k - \boldsymbol{\mu}_n), \quad (72)$$

for $1 \leq k, n \leq N$. Note that $\vartheta_{(n-1)N+k}^h(\mathbf{x})$ and $\vartheta_{N^2+(n-1)N+k}^h(\mathbf{x})$ are similarly computed.

Next, we express $u_{N,M}(\boldsymbol{\mu}) = \sum_{n=1}^N \alpha_{N,M,n}(\boldsymbol{\mu})\zeta_n$ and choose test functions $v = \zeta_j$, $1 \leq j \leq N$, in (69), we obtain the nonlinear algebraic system

$$\mathbf{E}_{N,M}^g \mathbf{g}_M(\boldsymbol{\alpha}_{N,M}(\boldsymbol{\mu}), \boldsymbol{\mu}) + \mathbf{E}_{N,M}^h \mathbf{h}_M(\boldsymbol{\alpha}_{N,M}(\boldsymbol{\mu}), \boldsymbol{\mu}) = \mu_1 \mathbf{F}_N, \quad (73)$$

where $\mathbf{E}_{N,M}^g = \mathbf{C}_{N,M}^g [\mathbf{B}_M^g]^{-1}$ and $\mathbf{E}_{N,M}^h = \mathbf{C}_{N,M}^h [\mathbf{B}_M^h]^{-1}$, for $1 \leq j \leq N$ and $1 \leq m, k \leq M$, we have

$$C_{N,M,jm}^g = \int_{\Omega} \psi_m^g \frac{\partial \zeta_j}{\partial x_1}, \quad C_{N,M,jm}^h = \int_{\Omega} \psi_m^h \frac{\partial \zeta_j}{\partial x_2} \quad (74)$$

and

$$\begin{aligned} g_{M,k}(\boldsymbol{\alpha}_{N,M}(\boldsymbol{\mu}), \boldsymbol{\mu}) &= g \left(\sum_{n=1}^N \alpha_{N,M,n}(\boldsymbol{\mu}) \zeta_n(\widehat{\mathbf{x}}_k^g), \boldsymbol{\mu} \right), \\ h_{M,k}(\boldsymbol{\alpha}_{N,M}(\boldsymbol{\mu}), \boldsymbol{\mu}) &= h \left(\sum_{n=1}^N \alpha_{N,M,n}(\boldsymbol{\mu}) \zeta_n(\widehat{\mathbf{x}}_k^h), \boldsymbol{\mu} \right). \end{aligned} \quad (75)$$

Note that $\mathbf{E}_{N,M}^g$, $\mathbf{E}_{N,M}^h$, and \mathbf{F}_N can be pre-computed in the offline stage since they are independent of $\boldsymbol{\mu}$.

We use Newton method to linearize (73) at a given iterate $\bar{\boldsymbol{\alpha}}_{N,M}(\boldsymbol{\mu})$ to arrive at the following linear system

$$\begin{aligned} (\mathbf{E}_{N,M}^g \mathbf{H}_{M,N}^g(\bar{\boldsymbol{\alpha}}_{N,M}(\boldsymbol{\mu}), \boldsymbol{\mu}) + \mathbf{E}_{N,M}^h \mathbf{H}_{M,N}^h(\bar{\boldsymbol{\alpha}}_{N,M}(\boldsymbol{\mu}), \boldsymbol{\mu})) \delta \boldsymbol{\alpha}_{N,M}(\boldsymbol{\mu}) = \\ \mu_1 \mathbf{F}_N - \mathbf{E}_{N,M}^g \mathbf{g}_M(\bar{\boldsymbol{\alpha}}_{N,M}(\boldsymbol{\mu}), \boldsymbol{\mu}) - \mathbf{E}_{N,M}^h \mathbf{h}_M(\bar{\boldsymbol{\alpha}}_{N,M}(\boldsymbol{\mu}), \boldsymbol{\mu}) \end{aligned} \quad (76)$$

where, for $1 \leq i \leq N$ and $1 \leq k \leq M$, we have

$$\begin{aligned} H_{M,N,ki}^g(\bar{\boldsymbol{\alpha}}_{N,M}(\boldsymbol{\mu}), \boldsymbol{\mu}) &= g'_u \left(\sum_{n=1}^N \bar{\alpha}_{N,M,n}(\boldsymbol{\mu}) \zeta_n(\widehat{\mathbf{x}}_k), \boldsymbol{\mu} \right) \zeta_i(\widehat{\mathbf{x}}_k), \\ H_{M,N,ki}^h(\bar{\boldsymbol{\alpha}}_{N,M}(\boldsymbol{\mu}), \boldsymbol{\mu}) &= h'_u \left(\sum_{n=1}^N \bar{\alpha}_{N,M,n}(\boldsymbol{\mu}) \zeta_n(\widehat{\mathbf{x}}_k), \boldsymbol{\mu} \right) \zeta_i(\widehat{\mathbf{x}}_k). \end{aligned} \quad (77)$$

Once the Newton iteration converges, we evaluate the RB output as

$$s_{N,M}(\boldsymbol{\mu}) = \sum_{n=1}^N \alpha_{N,M,n}(\boldsymbol{\mu}) L_{N,n} \quad (78)$$

where $L_{N,n} = \int_{\Omega} \zeta_n$ are pre-computed in the offline stage. The complexity of solving the linear system (76) per Newton iteration is $O(MN^2)$. Therefore, the RB approximation via empirical interpolation is efficient.

4.4. Numerical results

We present numerical results for the model problem of Section 4.1. The first-order EIM results reported herein are obtained by using the FOEIM Algorithm I. The parameter test sample S_{Test}^g is a uniform grid of size $N_{\text{Test}} = 30 \times 30$. We present in Figure 6 $\bar{\epsilon}_N^s$, $\bar{\epsilon}_{N,M}^s$, $\bar{\epsilon}_N^u$, and $\bar{\epsilon}_{N,M}^u$ as a function of N and in Table 5 $\bar{\eta}_{N,M}^s$ and $\bar{\eta}_{N,M}^u$ as a function of N . These quantities were defined in Section 3.4. As M increases, $\bar{\epsilon}_{N,M}^s$ (respectively, $\bar{\epsilon}_{N,M}^u$) converges to $\bar{\epsilon}_N^s$ (respectively, $\bar{\epsilon}_N^u$). The RB approximation based on the first-order EIM with $M = 3N$ is almost as accurate as the standard RB approximation, whereas the RB approximation based on the original EIM is significantly less accurate than the standard RB approximation. We observe that the average effectivities decrease toward unity as M increases. Furthermore, the first-order EIM with $M = 3N$ yields significantly smaller output effectivities than the original EIM for the same dimension N . Hence, the first-order EIM provides more accurate reduced basis approximation than the original EIM.

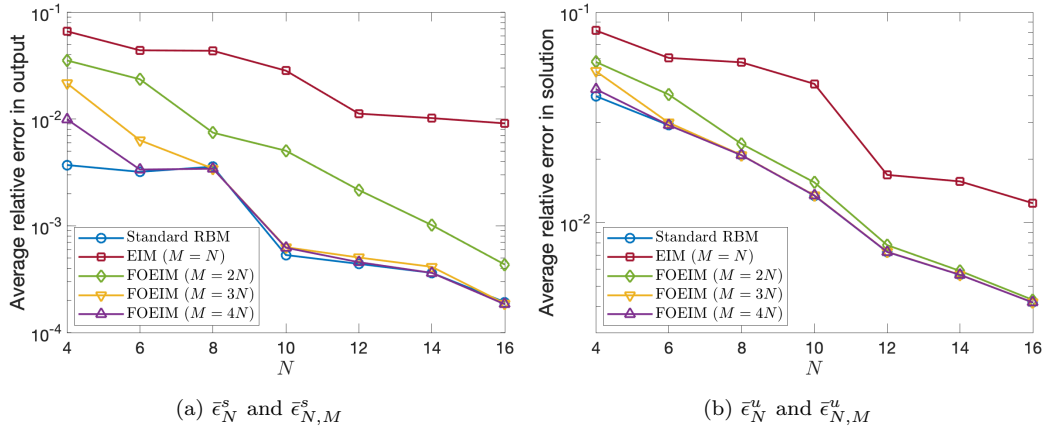


Figure 6: Convergence of the average relative error in output (a) and solution (b) for the model problem of Section 4.1.

We present in Table 6 the online computational times to calculate $s_N(\boldsymbol{\mu})$ and $s_{N,M}(\boldsymbol{\mu})$ as a function of N . The values are normalized with respect to the computational time for the direct calculation of the truth approximation output $s(\boldsymbol{\mu})$. The computational saving is significant: for an relative accuracy of less than 0.001 ($N = 10$, $M = 30$) in the output, the reduction in online cost is more than a factor of 2600; this is mainly because the matrix assembly of the nonlinear terms for the truth approximation is computationally very expensive. The standard RB approximation is 2 times faster the

N	$M = N$		$M = 2N$		$M = 3N$		$M = 4N$	
	$\bar{\eta}_{N,M}^s$	$\bar{\eta}_{N,M}^u$	$\bar{\eta}_{N,M}^s$	$\bar{\eta}_{N,M}^u$	$\bar{\eta}_{N,M}^s$	$\bar{\eta}_{N,M}^u$	$\bar{\eta}_{N,M}^s$	$\bar{\eta}_{N,M}^u$
4	56.61	2.20	37.10	1.56	27.67	1.43	12.28	1.17
6	22.17	2.21	16.38	1.33	2.46	1.02	1.21	1.00
8	55.05	2.94	6.72	1.12	1.31	1.00	1.12	1.00
10	346.71	4.53	63.51	1.11	6.38	1.01	3.47	1.00
12	94.53	3.02	14.00	1.11	1.75	1.00	1.41	1.00
14	139.88	3.55	6.67	1.06	1.57	1.00	1.06	1.00
16	252.99	3.78	9.31	1.04	1.49	1.00	1.10	1.00

Table 5: Average effectivities for the model problem of Section 4.1. The column with $M = N$ corresponds to the original EIM, while the columns with $M > N$ correspond to the first-order EIM.

truth FE approximation, but 1000 times slower than the RB approximation via empirical interpolation. The first-order EIM yields as accurate approximation as the standard RB method and reduces the online computational times by several orders of magnitude.

N	FEM	RBM	EIM	FOEIM	FOEIM	FOEIM
	$s(\boldsymbol{\mu})$	$s_N(\boldsymbol{\mu})$	$M = N$	$M = 2N$	$M = 3N$	$M = 4N$
4	1	5.15e-1	2.08e-4	2.23e-4	2.09e-4	2.00e-4
6	1	5.36e-1	2.37e-4	2.56e-4	2.45e-4	2.52e-4
8	1	5.53e-1	2.55e-4	2.81e-4	2.82e-4	3.01e-4
10	1	5.55e-1	2.76e-4	3.18e-4	3.25e-4	3.82e-4
12	1	5.63e-1	2.99e-4	3.36e-4	3.81e-4	4.28e-4
14	1	5.83e-1	3.29e-4	3.86e-4	4.44e-4	5.59e-4
16	1	5.89e-1	3.46e-4	4.09e-4	4.75e-4	6.14e-4

Table 6: Online computational times (normalized with respect to the time to solve for $s(\boldsymbol{\mu})$) for the model problem of Section 3.1.

5. Conclusion

We have presented an efficient model reduction technique for constructing accurate reduced-basis approximation of nonlinear PDEs via the first-order empirical interpolation. Although we apply our approach to elliptic problems, it can be extended to other PDEs with minor modification. Numerical results were presented to demonstrate that the first-order EIM approach provides computational savings of many orders of magnitude relative to the FE

approximation and the standard RB approximation. Furthermore, the first-order EIM approach is considerably more accurate than the original EIM approach for the same dimension of the RB space N . Indeed, the proposed approach can be made as accurate as the standard RB approximation by increasing the number of the interpolation points.

In this paper, we have not considered the selection of parameter sample sets and *a posteriori* error estimation. The accuracy, efficiency, and reliability of a reduced-order model depend crucially on a parameter sample set to guarantee rapid convergence, and *a posteriori* estimator [62, 63] to quantify the approximation error. If *a posteriori* error estimates are available, they can be used to select the parameter points by using the greedy sampling method [12, 64]. Therefore, *a posteriori* error estimation is an important topic to be addressed in future work. We would like to point out that *a posteriori* error estimation procedures have been successfully developed for nonlinear elliptic PDEs [40] and nonlinear parabolic PDEs [65]. *A posteriori* error estimation for nonlinear hyperbolic PDEs is an active yet challenging area of research. We would like to pursue dual-weighted residual error estimation [6, 66, 67] for nonlinear hyperbolic PDEs in future work.

It is natural to extend the proposed method to higher-order derivative information such as second-order partial derivatives. We believe that the use of higher-order partial derivatives may be necessary for nonlinear hyperbolic PDEs as it may improve the accuracy and stability of ROMs compared to the use of first-order derivatives. We leave this topic for future research.

Acknowledgements

We would like to thank Professor Anthony T. Patera at MIT, Professor Robert M. Freund at MIT, and Professor Yvon Maday at University of Paris VI for fruitful discussions. We gratefully acknowledge a Seed Grant from the MIT Portugal Program, the United States Department of Energy under contract DE-NA0003965 and the Air Force Office of Scientific Research under Grant No. FA9550-22-1-0356 for supporting this work.

References

- [1] C. W. Rowley, T. Colonius, R. M. Murray, Model reduction for compressible flows using POD and Galerkin projection, *Physica D. Nonlinear Phenomena* 189 (1-2) (2004) 115–129.

- [2] P. A. LeGresley, J. J. Alonso, Airfoil design optimization using reduced order models based on proper orthogonal decomposition, in: Fluids 2000 Conference and Exhibit, 2000, p. 2545. doi:10.2514/6.2000-2545.
- [3] D. J. Knezevic, N. C. Nguyen, A. T. Patera, Reduced basis approximation and a posteriori error estimation for the parametrized unsteady Boussinesq equations, *Mathematical Models and Methods in Applied Sciences* 21 (7) (2011) 1415–1442. doi:10.1142/S0218202511005441.
- [4] S. Lorenzi, A. Cammi, L. Luzzi, G. Rozza, POD-Galerkin method for finite volume approximation of Navier–Stokes and RANS equations, *Computer Methods in Applied Mechanics and Engineering* 311 (2016) 151–179. doi:10.1016/j.cma.2016.08.006.
- [5] M. Yano, Discontinuous Galerkin reduced basis empirical quadrature procedure for model reduction of parametrized nonlinear conservation laws, *Advances in Computational Mathematics* 45 (5-6) (2019) 2287–2320. doi:10.1007/s10444-019-09710-z.
- [6] M. Yano, Goal-oriented model reduction of parametrized nonlinear partial differential equations: Application to aerodynamics, *International Journal for Numerical Methods in Engineering* 121 (23) (2020) 5200–5226. doi:10.1002/nme.6395.
- [7] P. J. Blonigan, F. Rizzi, M. Howard, J. A. Fike, K. T. Carlberg, Model reduction for steady hypersonic aerodynamics via conservative manifold least-squares Petrov–Galerkin projection, *AIAA Journal* 59 (4) (2021) 1296–1312. doi:10.2514/1.J059785.
- [8] J. Yu, J. S. Hesthaven, Model order reduction for compressible flows solved using the discontinuous Galerkin methods, *Journal of Computational Physics* 468 (2022) 111452. doi:10.1016/j.jcp.2022.111452.
- [9] F. Ballarin, G. Rozza, POD–Galerkin monolithic reduced order models for parametrized fluid-structure interaction problems, *International Journal for Numerical Methods in Fluids* 82 (12) (2016) 1010–1034. doi:10.1002/flid.4252.
- [10] K. Carlberg, C. Farhat, J. Cortial, D. Amsallem, The GNAT method for nonlinear model reduction: Effective implementation and application to computational fluid dynamics and turbulent flows, *Journal of*

- Computational Physics 242 (2013) 623–647. [arXiv:1207.1349](#), [doi:10.1016/j.jcp.2013.02.028](#).
- [11] E. Du, M. Yano, Efficient hyperreduction of high-order discontinuous Galerkin methods: Element-wise and point-wise reduced quadrature formulations, *Journal of Computational Physics* 466 (2022) 111399. [doi:10.1016/j.jcp.2022.111399](#).
- [12] G. Rozza, D. B. P. Huynh, A. T. Patera, Reduced basis approximation and a posteriori error estimation for affinely parametrized elliptic coercive partial differential equations: Application to transport and continuum mechanics, *Archives Computational Methods in Engineering* 15 (4) (2008) 229–275.
- [13] D. B. Huynh, A. T. Patera, Reduced basis approximation and a posteriori error estimation for stress intensity factors, *International Journal for Numerical Methods in Engineering* 72 (10) (2007) 1219–1259. [doi:10.1002/nme.2090](#).
- [14] C. Farhat, P. Avery, T. Chapman, J. Cortial, Dimensional reduction of nonlinear finite element dynamic models with finite rotations and energy-based mesh sampling and weighting for computational efficiency, *International Journal for Numerical Methods in Engineering* 98 (9) (2014) 625–662. [doi:10.1002/nme.4668](#).
- [15] C. Farhat, T. Chapman, P. Avery, Structure-preserving, stability, and accuracy properties of the energy-conserving sampling and weighting method for the hyper reduction of nonlinear finite element dynamic models, *International Journal for Numerical Methods in Engineering* 102 (5) (2015) 1077–1110. [doi:10.1002/nme.4820](#).
- [16] P. Tiso, D. J. Rixen, Discrete empirical interpolation method for finite element structural dynamics, in: *Conference Proceedings of the Society for Experimental Mechanics Series*, Vol. 1, 2013, pp. 203–212.
- [17] Y. Chen, J. S. Hesthaven, Y. Maday, J. Rodríguez, Certified Reduced Basis Methods and Output Bounds for the Harmonic Maxwell’s Equations, *SIAM Journal on Scientific Computing* 32 (2) (2010) 970–996. [doi:10.1137/09075250X](#).

- [18] F. Vidal-Codina, N. C. Nguyen, J. Peraire, Computing parametrized solutions for plasmonic nanogap structures, *Journal of Computational Physics* 366 (2018) 89–106. [arXiv:1710.06539](#), [doi:10.1016/j.jcp.2018.04.009](#).
- [19] J. Pomplun, F. Schmidt, Accelerated a posteriori error estimation for the reduced basis method with application to 3d electromagnetic scattering problems, *SIAM Journal on Scientific Computing* 32 (2) (2010) 498–520. [doi:10.1137/090760271](#).
- [20] A. Manzoni, A. Quarteroni, G. Rozza, Shape optimization for viscous flows by reduced basis methods and free-form deformation, *International Journal for Numerical Methods in Fluids* 70 (5) (2012) 646–670. [doi:10.1002/flid.2712](#).
- [21] E. Qian, M. Grepl, K. Veroy, K. Willcox, A Certified Trust Region Reduced Basis Approach to PDE-Constrained Optimization, *SIAM Journal on Scientific Computing* 39 (5) (2017) S434–S460. [doi:10.1137/16m1081981](#).
- [22] K. Hoang, B. Khoo, G. Liu, N. Nguyen, A. Patera, Rapid identification of material properties of the interface tissue in dental implant systems using reduced basis method, *Inverse Problems in Science and Engineering* 21 (8) (2013) 1310–1334. [doi:10.1080/17415977.2012.757315](#).
- [23] N. C. Nguyen, G. Rozza, D. B. Huynh, A. T. Patera, Reduced basis approximation and a posteriori error estimation for parametrized parabolic pdes: Application to real-time bayesian parameter estimation, in: Biegler, Biros, Ghattas, Heinkenschloss, Keyes, Mallick, Tenorio, van Bloemen Waanders, Willcox (Eds.), *Large-Scale Inverse Problems and Quantification of Uncertainty*, John Wiley and Sons, UK, 2010, pp. 151–177. [doi:10.1002/9780470685853.ch8](#).
- [24] D. Galbally, K. Fidkowski, K. Willcox, O. Ghattas, Non-linear model reduction for uncertainty quantification in large-scale inverse problems, *International Journal for Numerical Methods in Engineering* 81 (12) (2010) 1581–1608. [doi:10.1002/nme.2746](#).
- [25] C. Lieberman, K. Willcox, O. Ghattas, Parameter and state model reduction for large-scale statistical inverse problems, *SIAM Journal on Scientific Computing* 32 (5) (2010) 2523–2542. [doi:10.1137/090775622](#).

- [26] N. C. Nguyen, A multiscale reduced-basis method for parametrized elliptic partial differential equations with multiple scales, *Journal of Computational Physics* 227 (23) (2008) 9807–9822.
- [27] E. Bader, M. Kärcher, M. A. Grepl, K. Veroy, Certified reduced basis methods for parametrized distributed elliptic optimal control problems with control constraints, *SIAM Journal on Scientific Computing* 38 (6) (2016) A3921–A3946. doi:10.1137/16M1059898.
- [28] M. Kärcher, Z. Tokoutsi, M. A. Grepl, K. Veroy, Certified Reduced Basis Methods for Parametrized Elliptic Optimal Control Problems with Distributed Controls, *Journal of Scientific Computing* 75 (1) (2018) 276–307. doi:10.1007/s10915-017-0539-z.
- [29] M. Kärcher, S. Boyaval, M. A. Grepl, K. Veroy, Reduced basis approximation and a posteriori error bounds for 4D-Var data assimilation, *Optimization and Engineering* 19 (3) (2018) 663–695. arXiv:1802.02328, doi:10.1007/s11081-018-9389-2.
- [30] Y. Maday, O. Mula, A generalized empirical interpolation method: Application of reduced basis techniques to data assimilation, in: *Springer INdAM Series*, Vol. 4, Springer, 2013, pp. 221–235. arXiv:1512.00683, doi:10.1007/978-88-470-2592-9-13.
- [31] Y. Maday, A. T. Patera, J. D. Penn, M. Yano, A parameterized-background data-weak approach to variational data assimilation: Formulation, analysis, and application to acoustics, *International Journal for Numerical Methods in Engineering* 102 (5) (2015) 933–965. doi:10.1002/nme.4747.
- [32] C. Prud’homme, D. Rovas, K. Veroy, Y. Maday, A. T. Patera, G. Turinici, Reliable real-time solution of parametrized partial differential equations: Reduced-basis output bounds methods, *Journal of Fluids Engineering* 124 (1) (2002) 70–80.
- [33] N. C. Nguyen, G. Rozza, A. T. Patera, Reduced basis approximation and a posteriori error estimation for the time-dependent viscous Burgers’ equation, *Calcolo* 46 (3) (2009) 157–185. doi:10.1007/s10092-009-0005-x.

- [34] M. A. Grepl, Y. Maday, N. C. Nguyen, A. T. Patera, Efficient reduced-basis treatment of nonaffine and nonlinear partial differential equations, *Mathematical Modelling and Numerical Analysis* 41 (3) (2007) 575–605. doi:10.1051/m2an:2007031.
- [35] N. C. Nguyen, J. Peraire, An efficient reduced-order modeling approach for non-linear parametrized partial differential equations, *International Journal for Numerical Methods in Engineering* 76 (1) (2008) 27–55. doi:10.1002/nme.2309.
- [36] D. S. Weile, E. Michielssen, K. Gallivan, Reduced-order modeling of multiscreen frequency-selective surfaces using Krylov-based rational interpolation, *IEEE Transactions on Antennas and Propagation* 49 (5) (2001) 801–813. doi:10.1109/8.929635.
- [37] J. R. Phillips, Projection-based approaches for model reduction of weakly nonlinear, time-varying systems, *IEEE Transactions on Computer-Aided Design of Integrated Circuits and Systems* 22 (2) (2003) 171–187. doi:10.1109/TCAD.2002.806605.
- [38] M. Rewieński, J. White, A trajectory piecewise-linear approach to model order reduction and fast simulation of nonlinear circuits and micromachined devices, *IEEE Transactions on Computer-Aided Design of Integrated Circuits and Systems* 22 (2) (2003) 155–170. doi:10.1109/TCAD.2002.806601.
- [39] M. Barrault, Y. Maday, N. C. Nguyen, A. T. Patera, An ‘empirical interpolation’ method: application to efficient reduced-basis discretization of partial differential equations, *Comptes Rendus Mathématique* 339 (9) (2004) 667–672. doi:10.1016/j.crma.2004.08.006.
- [40] N. C. Nguyen, A posteriori error estimation and basis adaptivity for reduced-basis approximation of nonaffine-parametrized linear elliptic partial differential equations, *Journal of Computational Physics* 227 (2) (2007) 983–1006. doi:10.1016/j.jcp.2007.08.031.
- [41] M. Drohmann, B. Haasdonk, M. Ohlberger, Reduced basis approximation for nonlinear parametrized evolution equations based on empirical operator interpolation, *SIAM Journal on Scientific Computing* 34 (2) (2012) A937–A969. doi:10.1137/10081157X.

- [42] J. S. Hesthaven, B. Stamm, S. Zhang, Efficient greedy algorithms for high-dimensional parameter spaces with applications to empirical interpolation and reduced basis methods, *ESAIM: Mathematical Modelling and Numerical Analysis* 48 (1) (2014) 259–283. doi:10.1051/m2an/2013100.
- [43] J. S. Hesthaven, C. Pagliantini, G. Rozza, Reduced basis methods for time-dependent problems, *Acta Numerica* 31 (2022) 265–345. doi:10.1017/S0962492922000058.
- [44] Y. Chen, S. Gottlieb, L. Ji, Y. Maday, An EIM-degradation free reduced basis method via over collocation and residual hyper reduction-based error estimation, *Journal of Computational Physics* 444 (2021) 110545. doi:10.1016/j.jcp.2021.110545.
- [45] N. C. Nguyen, A. T. Patera, J. Peraire, A 'best points' interpolation method for efficient approximation of parametrized functions, *International Journal for Numerical Methods in Engineering* 73 (4) (2008) 521–543. doi:10.1002/nme.2086.
- [46] B. Kramer, K. E. Willcox, Nonlinear model order reduction via lifting transformations and proper orthogonal decomposition, *AIAA Journal* 57 (6) (2019) 2297–2307. arXiv:1808.02086, doi:10.2514/1.J057791.
- [47] M. Yano, A. T. Patera, An LP empirical quadrature procedure for reduced basis treatment of parametrized nonlinear PDEs, *Computer Methods in Applied Mechanics and Engineering* 344 (2019) 1104–1123. doi:10.1016/j.cma.2018.02.028.
- [48] S. Chaturantabut, D. C. Sorensen, Nonlinear model reduction via discrete empirical interpolation, *SIAM Journal on Scientific Computing* 32 (5) (2010) 2737–2764. doi:10.1137/090766498.
- [49] J. Maierhofer, D. J. Rixen, Model order reduction using hyperreduction methods (DEIM, ECSW) for magnetodynamic FEM problems, *Finite Elements in Analysis and Design* 209 (2022) 103793. doi:10.1016/j.finel.2022.103793.
- [50] P. Astrid, S. Weiland, K. Willcox, T. Backx, Missing point estimation in models described by proper orthogonal decomposition, *IEEE*

- Transactions on Automatic Control 53 (10) (2008) 2237–2251. doi:10.1109/TAC.2008.2006102.
- [51] B. Peherstorfer, Z. Drmac, S. Gugercin, Stability of discrete empirical interpolation and gappy proper orthogonal decomposition with randomized and deterministic sampling points, *SIAM Journal on Scientific Computing* 42 (5) (2020) A2837–A2864. arXiv:1808.10473, doi:10.1137/19M1307391.
- [52] J. L. Eftang, B. Stamm, Parameter multi-domain ‘hp’ empirical interpolation, *International Journal for Numerical Methods in Engineering* 90 (4) (2012) 412–428. doi:10.1002/nme.3327.
- [53] B. Peherstorfer, D. Butnaru, K. Willcox, H. J. Bungartz, Localized discrete empirical interpolation method, *SIAM Journal on Scientific Computing* 36 (1) (2014). doi:10.1137/130924408.
- [54] R. Everson, L. Sirovich, Karhunen-Loeve procedure for gappy data, *Opt. Soc. Am. A* 12 (8) (1995) 1657–1664.
- [55] K. Willcox, Unsteady Flow Sensing and Estimation via the Gappy Proper Orthogonal Decomposition, *Computers and Fluids* 35 (2006) 208–226.
- [56] R. Zimmermann, K. Willcox, An accelerated greedy missing point estimation procedure, *SIAM Journal on Scientific Computing* 38 (5) (2016) A2827–A2850. doi:10.1137/15M1042899.
- [57] J. P. Argaud, B. Bouriquet, H. Gong, Y. Maday, O. Mula, Stabilization of (G)EIM in Presence of Measurement Noise: Application to Nuclear Reactor Physics, in: *Lecture Notes in Computational Science and Engineering*, Vol. 119, 2017, pp. 133–145. arXiv:1611.02219.
- [58] P. Guillaume, M. Masmoudi, Solution to the time-harmonic Maxwell’s equations in a waveguide: use of higher-order derivatives for solving the discrete problem, *SIAM J. Numer. Anal.* 34 (4) (1997) 1306–1330.
- [59] K. Ito, S. S. Ravindran, A Reduced Basis Method for Control Problems Governed by {PDEs}, in: W. Desch, F. Kappel, K. Kunisch (Eds.), *Control and Estimation of Distributed Parameter Systems*, Birkhäuser, 1998, pp. 153–168.

- [60] Y. Maday, N. C. Nguyen, A. T. Patera, G. S. Pau, A general multipurpose interpolation procedure: The magic points, *Communications on Pure and Applied Analysis* 8 (1) (2009) 383–404. doi:10.3934/cpaa.2009.8.383.
- [61] J. Vila-Pérez, R. L. Van Heyningen, N.-C. Nguyen, J. Peraire, Exasim: Generating discontinuous Galerkin codes for numerical solutions of partial differential equations on graphics processors, *SoftwareX* 20 (2022) 101212. doi:https://doi.org/10.1016/j.softx.2022.101212.
- [62] D. B. P. Huynh, G. Rozza, S. Sen, A. T. Patera, A successive constraint linear optimization method for lower bounds of parametric coercivity and inf-sup stability constants, *C. R. Acad. Sci. Paris, Analyse Numérique* 345 (8) (2007) 473–478.
- [63] S. Sen, K. Veroy, D. B. P. Huynh, S. Deparis, N. C. Nguyen, A. T. Patera, Natural norm” a posteriori error estimators for reduced basis approximations, *Journal of Computational Physics* 217 (1) (2006) 37–62. doi:10.1016/j.jcp.2006.02.012.
- [64] S. Boyaval, C. L. Bris, Y. Maday, N. C. Nguyen, A. T. Patera, A reduced basis approach for variational problems with stochastic parameters: Application to heat conduction with variable Robin coefficient, *Computer Methods in Applied Mechanics and Engineering* 198 (41-44) (2009) 3187–3206. doi:10.1016/j.cma.2009.05.019.
- [65] M. Grepl, Reduced-Basis Approximations and $\{ \em A Posteriori \}$ Error Estimation for Parabolic Partial Differential Equations, Ph.D. thesis, Massachusetts Institute of Technology, Cambridge, MA (may 2005).
- [66] P. J. Blonigan, E. J. Parish, Evaluation of dual-weighted residual and machine learning error estimation for projection-based reduced-order models of steady partial differential equations, *Computer Methods in Applied Mechanics and Engineering* 409 (2023) 115988. doi:10.1016/j.cma.2023.115988.
- [67] E. Du, M. Sleeman, Adaptive Discontinuous-Galerkin Reduced-Basis Reduced-Quadrature Method for Many-Query CFD Problems, in: *AIAA Aviation and Aeronautics Forum and Exposition, AIAA AVIATION Forum 2021*, 2021, pp. AIAA–2021–2716. doi:10.2514/6.2021-2716.